

HYDROGENATION OF GRAPHENE ON Ir(111) BY VIBRATIONALLY EXCITED MOLECULES



AARHUS
UNIVERSITET

Anders Christian Løchte Jørgensen - 201304162
iNano, Aarhus University

Supervisor:
Liv Hornekær
Department of Physics and Astronomy, Aarhus University
June 2016

Abstract

The hydrogenation of graphene on Ir(111) using vibrationally excited molecules has been studied. vibrationally excited D₂ molecules with an energy exceeding the dissociation energy of D₂ on graphene are produced by associative recombination of atomic hydrogen on chamber walls. This implies that vibrational levels of at least $v''=7$ are achieved. Atomic hydrogen was produced using a hydrogen atom beam source (HABS), operating at temperatures of 1343°C, 1593°C and 1745°C. Having a D₂ chamber pressure of $5 \cdot 10^{-7}$ mbar during dosing, it was found that the fraction of hydrogenated moiré super cells on graphene after 20 min D₂ exposure were; 35%, 28%, and a few % with HABS temperatures of 1745°C, 1593°C and 1343°C, respectively. Furthermore, the graphene/Ir(111) surface was saturated after 60 min exposure to excited molecules at 1745°C. The hydrogenated graphene/Ir(111) surface is examined by STM, and the observations show that hydrogen adsorption primarily happens at the FCC site of the moire unit cell. The periodicity of the hydrogenated surface is equal to the moiré periodicity of clean gaphene on Ir(111). In order to investigate the dissociation of D₂ further, temperature programmed desorption (TPD) measurements were carried out. These show that the desorption of hydrogen follows a first order desorption, with desorption energies of 2.1 ± 0.4 eV. Following exposure to excited molecules it is found that formation of hydrogen dimers is absent on the graphene on Ir(111) surface. However, dimer peaks appear following dosage of atomic hydrogen. Bilayered graphene patches were observed by STM. Images reveal that the hydrogenation of the bilayer patch is absent, due to its free standing graphene resemblance. Furthermore it is observed that a new kind of moiré pattern is present at bilayer patches with graphene sheets presumably rotated compared to each other.

Contents

| | | |
|----------|---|-----------|
| 1 | Introduction | 1 |
| 2 | Graphene | 2 |
| 2.1 | Graphene on Ir(111) | 3 |
| 2.2 | Hydrogenation of Graphene on Ir(111) Using Atomic Deuterium | 4 |
| 2.2.1 | Formation of vibrationally excited Deuterium | 5 |
| 3 | Techniques | 7 |
| 3.1 | Scanning Tunneling Microscopy - STM | 7 |
| 3.2 | Temperature Programmed Desorption - TPD | 8 |
| 3.3 | Low Energy Electron Diffraction - LEED | 10 |
| 4 | Experimental Approach | 11 |
| 4.1 | The Coal Chamber | 11 |
| 4.2 | STM Imaging and D ₂ Dosage | 12 |
| 4.2.1 | STM Calibration | 12 |
| 4.2.2 | D ₂ Dosage | 13 |
| 4.2.3 | Sample Annealing and Graphene Repair | 14 |
| 4.3 | TPD | 14 |
| 5 | Results | 17 |
| 5.1 | Graphene on Ir(111) | 17 |
| 5.2 | D ₂ on Graphene | 18 |
| 5.2.1 | Full Hydrogen Coverage | 19 |
| 5.2.2 | 1745°C Dose | 20 |
| 5.2.3 | 1593°C Dose | 21 |
| 5.2.4 | 1343°C Dose | 22 |
| 5.3 | TPD measurements | 23 |
| 5.3.1 | Atomic and molecular D ₂ - single layered sample | 23 |
| 5.4 | Graphene bilayered sample | 25 |
| 5.4.1 | TPD of bilayered sample | 25 |
| 5.4.2 | STM images of bilayers | 26 |
| 5.4.3 | LEED of bilayered sample | 27 |
| 6 | Conclusion and Future Perspectives | 29 |
| | Bibliography | 30 |

1

Introduction

With an ever rising demand of energy, the world is in need of great energy storage devices. Through the ages a wide range of these devices have been invented including electrochemical devices such as Li-ion batteries, electrical capacitors or mechanical flywheels. These are only some devices capable of storing energy. However, with a steadily increasing global average temperature, a cleaner and better way of storing energy is demanded. Research within hydrogen storage is therefore massive, since water is the only product from the combustion of hydrogen. Hydrogen has proven itself difficult to store at high hydrogen densities. Liquid hydrogen requires cryogenic tanks at a temperature around 20K. Using materials to store hydrogen instead is a promising solution to the hydrogen storage problem. One of such materials is graphene. Since graphene is one atom thick, its surface to volume ratio is very high. Therefore a high weight percent of stored hydrogen is obtainable. Furthermore the release of hydrogen from graphene can be controlled, and graphene does therefore show promising prospect.

This bachelor project aims at describing the hydrogenation of graphene using vibrationally excited molecules. A graphene on Ir(111) surface is chosen as the substrate. The surface is investigated under ultra-high vacuum conditions (UHV) by scanning tunneling microscopy (STM) and a qualitative description of the hydrogenation is explained with theoretical backing. Furthermore the desorption of hydrogen from the surface is investigated by temperature programmed desorption (TPD).

All of the experiments conducted in this bachelors thesis is done in the Surface Dynamics Lab during the first six months of 2016. I am grateful to Liv Hornekær for being a wonderful supervisor and giving me the opportunity to work in the lab. Furthermore PhD student Line Kyhl has been indispensable with guidance of using 'The Coal Chamber', as well as being supportive during the entire procedure. A big thanks to everyone in the Surface Dynamics Lab including; Richard Balog, Andrew Cassidy, Anders Lind Skov, Frederik Doktor, Susanne Halkjær, Uffe Holm and Kasper Medium Rasmussen. All of which have been helpful, kind and great company during this project. A special thanks goes to Antonija Grubisic Cabo for conducting the LEED experiments. The LEED setup will not be discussed in this report.

2

Graphene

Not only is carbon one of the key elements in every known life form, it also has a wide span of applications ranging from common lead in pencils to jewelry in the form of rare earth diamonds. Graphene has also been the subject of extensive research due to its fascinating qualities e.g. an electron mobility of $2.5 \cdot 10^5 \text{ cm}^2 \text{V}^{-1} \text{s}^{-1}$ [1] which is much greater than the mobility in typical metals of $50 \text{ cm}^2 \text{V}^{-1} \text{s}^{-1}$. [2] Furthermore, the Youngs modulus of graphene has been measured to 1 TPa and the intrinsic strength to 130 Gpa. [1] A thermal conductivity exceeding $3,000 \text{ W mK}^{-1}$, adds to the remarkable qualities of graphene.

Graphene is a two dimensional honeycomb lattice of carbon atoms. Each carbon atom is sp^2 hybridized where one s orbital and two p orbitals form three planar bonds with a separation angle of 120° . [3] The distance between the individual carbon atoms is 1.42 \AA . Due to the flexibility of the sp^2 bonds in the z direction, many other structures can be formed by a sheet of graphene, such as fullerenes, carbon nanotubes, and graphite. Fullerenes are the shape of balls, consisting of 60 carbon atoms. These balls are formed by wrapping up a sheet of graphene. The graphene sheet is wrapped up due to the formation of pentagons. Obviously, carbon nanotubes are tube-shaped and they are formed from the connection of two edges on a graphene sheet. Graphite is the structure arising, when multiple layers of graphene are stacked. At this point, only the Van Der Waals forces between the individual layers keep the layers in their places. All of these structures are shown in Figure 2.1. The graphene unit cell consists of only two lattice points, and the lattice vectors can be written as follows:

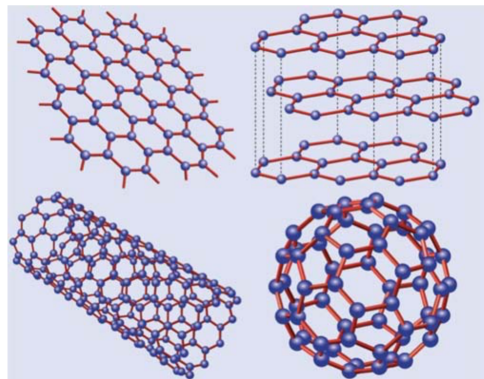


Figure 2.1: Graphic interpretation of the different structures derived from graphene. Top left shows a graphene monolayer beside a 3-layered graphite structure. Bottom left shows a carbon nanotube beside a C_{60} fullerene.

$$a_1 = \frac{a}{2}(3, -\sqrt{3}) \quad a_2 = \frac{a}{2}(3, \sqrt{3})$$

2.1 Graphene on Ir(111)

When a monolayer of graphene is synthesized on top of a metal surface, the underlying metal and the graphene monolayer rarely have identical lattice parameters. This results in a mismatch between the two layers causing the alignment to differ, which again leads to a phenomenon known as a moiré effect, where a superstructure appears from the two mismatching lattices.

These experiments study graphene on top of an Ir(111) surface. Ir crystallises as a face centered cubic lattice, and once cut in the [111] direction, the surface atoms have a hexagonal close packed arrangement. [4] The atomic diameter of Ir is 2.715 Å [4], which differs slightly from the value of the graphene lattice with a periodicity of 2.45 ± 0.04 Å [5], and the formation of a moiré pattern is therefore expected.

Graphene on Ir(111) has a well-defined moiré structure which is depicted in Figure 2.2a. Here the grey atoms show the Ir(111) surface, and the red layer on top corresponds to the graphene sheet. The moiré pattern is seen as bright spots across the surface where an Ir atom is found directly below the center of a graphene hexagon. It is seen from Figure 2.2a that the moiré pattern has a periodicity, and according to litterature the repeat vector has a length of 25.2 ± 0.4 Å. [5]

The graphene on Ir(111) moiré unit cell is outlined in Figure 2.2a, and a zoom of this is shown in Figure 2.2b. In the latter figure the ATOP, FCC and HCP positions are marked by circles. These areas within the unit cell are of special interest due to special alignments between the underlying Ir(111) atoms and the graphene sheet. The ATOP sites are positioned in the corners of the unit cell rhombus where an Ir atom is just below the center of a graphene hexagon. In these sites the distance to the underlying Ir(111) surface is slightly higher than the FCC and HCP sites, and therefore the sheet resemble free standing graphene. [6] In the HCP site, the graphene hexagon is aligned with the two underlying Ir layers as a HCP lattice. This means that an atom from the Ir(S-1) layer is directly under the center of a graphene hexagon, where S denotes the layer number starting from the uppermost. In the FCC site, an atom from the Ir(S-2) layer is directly under the center of a graphene hexagon. In both the HCP and FCC site, every second carbon atom is directly above an Ir atom. [7]

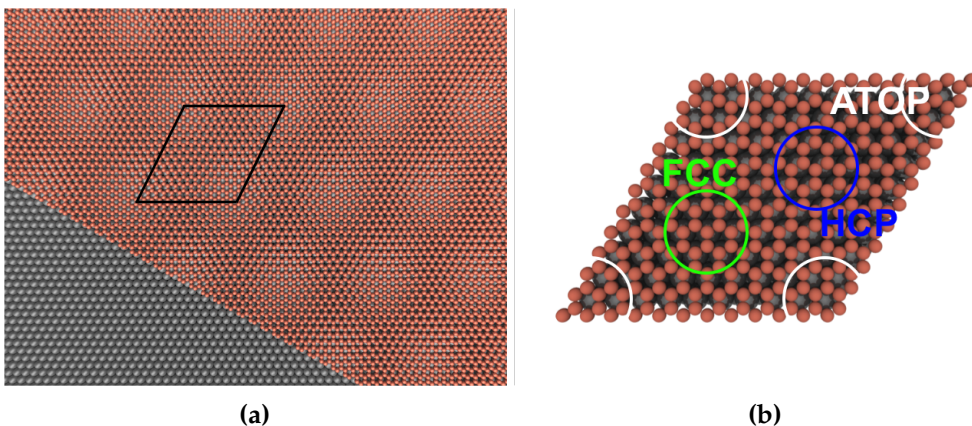


Figure 2.2: Graphic interpretation of graphene on Ir(111). (a) shows an Ir(111) (grey) surface with the moiré structure once the graphene sheet (red) is on top. (b) shows a moiré unit cell. [8]

2.2 Hydrogenation of Graphene on Ir(111) Using Atomic Deuterium

Chemical functionalization with different species drastically changes the properties of graphene. The underlying surface determines the adsorption of any species. In this bachelor's thesis the underlying surface is Ir(111). It is important to understand the process of adsorption of hydrogen to the Graphene on Ir(111), due to the special abilities arising from the functionalization of graphene by hydrogen. These effects include a bandgap opening of at least 450 meV. [9] The bandgap enables a large number of possibilities for the usage of functionalized graphene, where the most appealing is the construction of a new type of field effect transistors. Other forms of applications of functionalized graphene is within the area of energy storage. The one atom thick monolayer makes graphene a good choice when storing hydrogen due to the large surface to volume ratio. When hydrogen adsorbs to the graphene monolayer, the structural arrangement changes and the graphene undergoes a transition from sp^2 hybridization to sp^3 hybridization. This implies that the otherwise flat graphene sheet is distorted due to the 3-dimensional conformation of the bonds in the sp^3 hybridization. Every other carbon atom turns downwards and constructs a bond to the underlying Ir(111) surface. This is only possible in the HCP and FCC sites of the moiré unit cell where every other carbon atom of the graphene is situated directly above an Iridium atom. This indicate that the hydrogenation of graphene follows the moiré pattern. [6] As a result hereof, we expect the formation of a superstructure from the hydrogenated surface with the same periodicity as that of the moiré pattern.

A graphical interpretation of the hydrogenation of graphene on Ir(111) is shown in Figure 2.3, which is made by Line Kyhl. Here it is seen that clusters of hydrogen bind to the carbon atoms in the FCC and HCP sites. Figure 2.3b demonstrates how every other carbon atom binds to the Ir(111) surface and every other binds to a hydrogen atom. Furthermore, dimers of hydrogen are seen binding to the surface at the ATOP sites. In these regions, the distance to the Iridium is increased compared to the FCC and HCP sites. In these areas the graphene resembles free standing sheets and no bonds are formed between the Iridium and the carbon atoms.

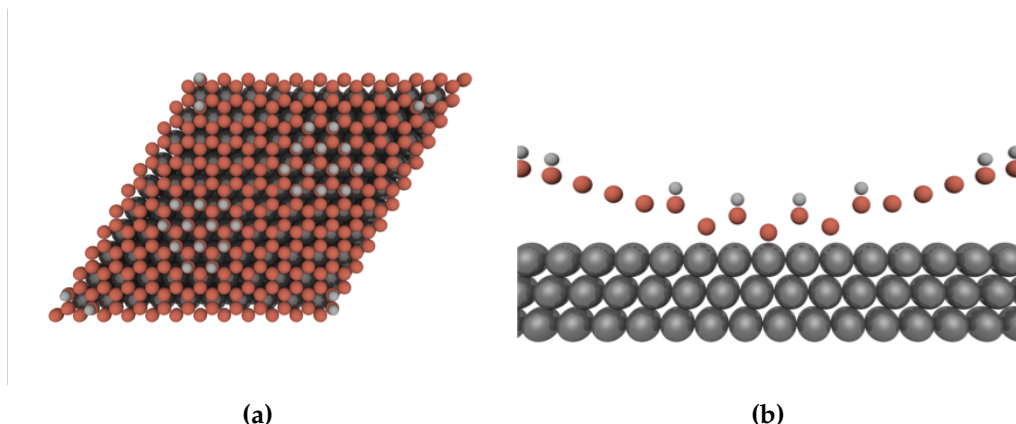


Figure 2.3: Graphic interpretation of the hydrogenation of graphene on Ir(111) by hot atoms. [8]

2.2.1 Formation of vibrationally excited deuterium

Vibrationally excited hydrogen molecules are produced when atoms from a gas phase recombine with atoms on the metal walls. This mechanism excite molecules to vibrational states as high as $v'' = 9$. [10] The vibrational states follow a boltzmann distribution at levels up to $v'' = 3$, and a non boltzmann distribution with an excess of excited states at higher levels. The distribution of excited molecules is seen in Figure 2.4, where the energies of the states are seen as well. The energy of a hydrogen molecule in the $v'' = 9$ state is 3.56 eV, which is enough to dissociate onto free standing graphene with an adsorption barrier ranging from 3.3 eV to 3.9 eV for relaxed graphene, and from 4.3 eV to 4.7 eV for unrelaxed graphene. [11] Furthermore recent DFT calculations have shown that the initial molecule need an energy of at least 3 eV to dissociate to graphene on Ir(111). However the distortion of the graphene sheet as the sp^2 to sp^3 hybridization undergoes reduce the barrier by 1 eV. This means that the following excited molecules only need an energy of at least 2 eV in order to dissociate to the graphene. [12]

The formation of vibrationally excited hydrogen molecules is limited by the amount of atomic hydrogen produced. By using a hot filament it is possible to dissociate hydrogen molecules on the filament surface, creating an atomic gas phase. When the dissociative surface has been heated, its coverage is very low and the fraction of a monolayer is in the order of $\theta < 10^{-4}$. [13] Therefore a valid assumption is that the hydrogen molecules from the gas phase are impinging on a clean surface. Based on this assumption the flux of atomic hydrogen from the surface is given by: [13]

$$\phi(H) = 2s_m P_a \phi(H_2) \quad (2.1)$$

Here s_m is the sticking probability of molecular hydrogen, and P_a is the atomization probability. $\phi(H_2)$ is the flux of molecular hydrogen towards the surface. The factor of 2 accounts for the two hydrogen atoms resulting from the dissociation of a single molecule. The sticking probability is a material and temperature dependant factor, and the flux of molecules towards the surface is a function of the pressure of the gas phase. The probability of atomization is given by the following: [13]

2.2. Hydrogenation of Graphene on Ir(111) Using Atomic Deuterium

$$P_a = \frac{1}{4} [\{(K_p/\gamma p)(K_p/\gamma p + 8)\}^{\frac{1}{2}} - K_p/\gamma p], \quad (2.2)$$

where K_p is the equilibrium constant of the atomization reaction, $\gamma = \sqrt{\frac{T_f}{T_g}}$, with subscripts indicating the temperatures of the filament and the gas, respectively. The gas pressure is p . This study investigates the hydrogenation of graphene on Ir(111), and estimates the hydrogenation threshold. By changing the amount of atomic hydrogen impinging the walls in the UHV chamber, the point at which no hydrogen is adsorbed to the graphene on Ir(111) surface can be found. During these experiments the gas pressure and the gas temperature are kept constant. Hence, the temperature of the hydrogen cracker is altered in order to determine the temperature, at which the number of excited molecules in the high vibrational levels, is close to zero.

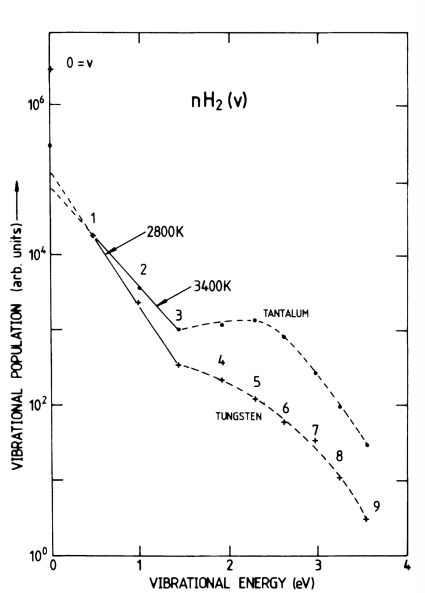


Figure 2.4: Distribution vibrationally excited H_2 molecules from recombinative desorption on chamber walls. The vibrational energy is seen on the x-axis.

3

Techniques

3.1 Scanning Tunneling Microscopy - STM

The main technique used in this study is scanning tunneling microscopy (STM), and more specifically the Aarhus STM. The Aarhus STM is an enhancement of the original version invented by Heinrich Rohrer and Gerhard Binnig in 1981. [14] The STM is used to create surface images with atomic resolution of conducting samples, which makes the technique irreplaceable in this study.

Images are made by scanning the sample surface with a very sharp metal tip. As the sample is scanned, the tunneling current between the tip and the sample is mapped in order to create an image of the surface. The high sensitivity of the STM stems from the tunneling transmittivity which depends exponentially on the distance between the tip and the sample. The distance between the surface and the tip is measured indirectly by the tunneling current which changes by a factor of approximately 10 for every ångstrøm. [15] A figure of the Aarhus STM is shown in Figure 3.1. The sample (1) is positioned within the Tantalum sample holder (2) and both are fixed with clamps (3). The STM tip held by a macor holder (5) is seen just above the sample (4), and this is controlled by the piezo scanner tube (6). In continuation of the scanner tube, a rod (7) is mounted which extends through another configuration of piezo elements called "The inchworm". This inchworm motor, held by another macor ring (8), is able to clamp to the rod and either expand or contract, in order to approach and retire the tip from the sample. The STM is thermally isolated from the rest of the environment by quartz balls (10). If, despite the thermal isolation, the temperature drops during cooling, a zener diode (11) heats up the STM.

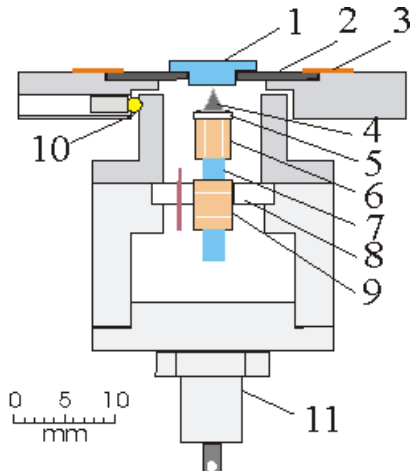


Figure 3.1: Schematic of the Aarhus STM. [14]

If the distance is too long, the electrons perceive a vacuum barrier which is too high and no tunneling occurs. As the distance between the sample and the tip is reduced, the probability of

an electron tunneling through the vacuum barrier increases until a certain point where tunneling happens. In order to achieve tunneling, the electrons need energy which at least equals the work function given by; $\phi = E_{vac} - E_F$, where E_{vac} is equal to the energy of the vacuum barrier and E_F is the energy at the fermi level. In order to keep a current flowing, a bias is applied between the sample and the tip. The energy of the fermi levels are altered by eV , where V is the voltage difference. This voltage difference establishes a constant flowing tunneling current, which can be calculated using the Wentzel-Kramers-Brillouin approximation. The tunneling current is given by: [16]

$$I = \int_0^{eV} \rho_s(E, r) \rho_t(E - eV, r) T(E, eV, r) dE, \quad (3.1)$$

where $\rho_s(E, r)$ and $\rho_t(E - eV, r)$ are the local densities of states (LDOS) of energy E at the position r . $T(E, eV, r)$ is the tunneling transmission probability for electrons with energy E and an applied voltage of eV . When the applied voltage, $eV < 0$, the sample is negatively biased, and when $eV > 0$ the sample is positively biased.

The tunneling transmission probability is given by the following: [16]

$$T(E, eV) = \exp \left(-\frac{2Z\sqrt{2m}}{\hbar} \sqrt{\frac{\phi_s + \phi_t}{2} + \frac{eV}{2} - E} \right), \quad (3.2)$$

where Z is the distance between the sample and the tip, and m is the mass of the electron. ϕ_s and ϕ_t are the work functions of the sample and the tip, respectively. From this expression it is seen that once the sample is negatively biased, the limits in equation 3.1 range from 0 to $eV < 0$. Equation 3.2 then returns the highest probability at $E = 0$, which expresses the energy at the fermi level of the sample. If, on the other hand, the sample has a positive bias, equation 3.1 has the limits 0 to $eV > 0$. Now equation 3.2 returns the highest probability at the energy $E = eV$, which is the energy at the fermi level of the tip. This means a negatively biased electrode always has the highest tunneling transmission probability, and the electrons always flow towards the positively biased electrode.

The tunneling current can be calculated, assuming that the density of states of the sample and the tip are constant, and that $eV \ll \phi_{s,t}$. [16,17]

$$I = \rho_s \rho_t V \exp \left(-\frac{2\sqrt{2(\phi_s + \phi_t)m}}{\hbar} Z \right). \quad (3.3)$$

This shows that the tunneling current as mentioned earlier depends exponentially on the distance to the sample. Furthermore, it is seen that the tunneling current depends on the bias applied, the LDOS of the sample and the tip, and their respective work functions.

3.2 Temperature Programmed Desorption - TPD

The desorption kinetics of hydrogen from the graphene on the Ir(111) surface is studied by use of temperature programmed desorption (TPD). Here the temperature of the sample is raised as a

3.2. Temperature Programmed Desorption - TPD

function of time. The temperature program, $\beta(t) = \frac{dT}{dt}$, is commonly a linear ramp with a rate ranging from 10^{-1} to 10^2 K s $^{-1}$. [18] The adsorption and desorption rates are studied by monitoring the time evolution of the coverage of the sample denoted θ . The coverage of a given adsorbate is given as the number of adsorbates on the surface as a percentage of the number of adsorbate sites. The time evolution of the coverage is naturally given by the rate of adsorption, R_a , subtracted by the rate of desorption. R_a is given by: [18]

$$R_a = \frac{S(\theta, T) P a_s}{\sqrt{2\pi m k_B T}} \quad (3.4)$$

For R_a ; the initial factor $S(\Theta, T)$ is the sticking factor, which is a substrate dependant function describing the probability of an adsorbate to stick to the surface. The rest of the equation describes the flux of atoms impinging the surface, and this expression is known as the Hertz-Knudsen equation. m is the mass of the adsorbing molecules, T is the gas temperature and k_B is Boltzmanns constant.

When conducting the TPD measurement the adsorbates desorb from the surface at a certain rate, until the surface is clean. The desorbed molecules are analysed by a quadropole mass analyzer. A typical evolution of the coverage and rate of desorption is seen in Figure 3.2 as well as a typical TPD curve measured by the quadropole. Here it is seen that the rate of desorption, in theory, rise exponentially with the temperature. In practice, however, the counts of desorbed molecules eventually fall off to zero, as the surface coverage approach zero. The number of desorbed molecules can be described by the Polanyi-Wigner equation, which is given by: [18, 20]

$$I(T) \sim -\frac{d\theta}{dt} = v(\theta, T) \cdot \theta^n \cdot \exp\left(\frac{-E_{des}(\theta, T)}{k_B T}\right), \quad (3.5)$$

where $I(T)$ is the number of molecules, and $v(\theta, T)$ is the exponential pre factor. Also n is the desorption order. Common desorption orders are, $n = 1$ describing molecular desorption, or $n = 2$ describing associative desorption where species recombine on the surface as they desorb. During these experiments it is assumed that hydrogen adsorbed to graphene on Ir(111) has a first order desorption rate. Redhead proposed a simple and applicable approach to TPD spectra from which the desorption energy can be calculated. [18] It is assumed that the desorption from the surface is of first order. Furthermore, the exponential pre factor as well as the desorption energy are assumed to be coverage independent. The energy of desorption is then approximated by the following: [21]

$$E_{des} \approx RT_P \left[\frac{vT_P}{\beta} - 3.64 \right] \quad (3.6)$$

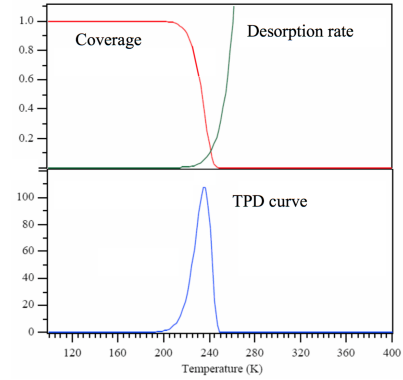


Figure 3.2: Top: Surface coverage and desorption rate. Bottom: Example of TPD curve. [19]

This equation is used to estimate the energy of desorption from the TPD measurements. A common exponential prefactor of $v = 10^{13} \text{ s}^{-1}$ is used. This factor might, however, vary between 10^{10} s^{-1} and 10^{20} s^{-1} [18]. This results in a significant error in the calculated energy of desorption of $\pm 20\%$. [21]

3.3 Low Energy Electron Diffraction - LEED

The first low energy electron diffraction (LEED) experiments were carried out by Clinton Davisson and Lester Germer in 1925 at Bell Labs in New York. Here sharp interference patterns from electron scattering from small millimeter sized nickel crystals were observed. This was only few years after De Broglie had postulated the wave nature of electrons. The wavelength of electrons is given by: [22]

$$\lambda_e = \frac{h}{m_e v} = \left(\frac{1.50 \text{ eV}}{E_{kin}} \right)^{1/2}, \quad (3.7)$$

with m_e as the electron mass, and v as the velocity. Given kinetic energies ranging from few tens to few hundreds eV, the wavelength is of the order of 1\AA , which is a typical interatomic distance. Using electron beams with these energies the crystal periodicity can therefore be determined by conducting LEED experiments. The technique is perfect for determining the surface geometries of samples since the inelastic mean free path of the electrons is around 1 nm. [22]

The basic principle of LEED is based on the elastic scattering of electrons. An electron beam with an energy, within the previously mentioned interval, is directed at the sample surface. Scattering of the electrons take place, and the pattern is visualised on a sensitive screen. A typical LEED setup is visualised in Figure 3.3. The wave vector of the diffracted electrons are given by the reciprocal lattice vectors of the sample surface:

$$k_{||,out}(n_1, n_2) = k_{||,in} + n_1 a_1^* + n_2 a_2^* \quad (3.8)$$

This only the component of the diffracted beam that is parallel to the incident beam. The z-component is given as:

$$k_{z,out}(n_1, n_2) = \left[\frac{2m_e E_{kin}}{h^2} - |k_{||,out}(n_1, n_2)|^2 \right]^{1/2} \quad (3.9)$$

In order to get a diffraction spot, the square root of the right hand side must be real. This means that the number of visual diffraction spots increases with the incident beam energy.

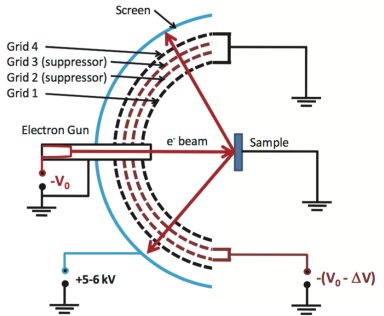


Figure 3.3: Graphic interpretation of a LEED setup. [22]

4

Experimental Approach

4.1 The Coal Chamber

The experiments are carried out under UHV conditions, with pressures around $1 \cdot 10^{-9}$ mbar. This is crucial because contaminants adsorb to the surface which ruins the quality of the data. The minimal amount of time needed to create a monolayer of contaminants on the surface can be calculated by the Hertz-Knudsen equation mentioned in chapter 3. It is assumed that the sticking coefficient equals 1, and that a monolayer require 10^{15} atoms pr. cm^2 . [23] Taking 10^{15} and dividing by the rate of impinging molecules on 1 cm^2 at 300 K, given by the Hertz-Knudsen equation, it is found that the time needed to create a monolayer of contaminants is inversely proportional to the pressure. A mass of 4 amu has been used as the mass of the impinging molecules.

$$t_{ML} = \frac{10^{19} \text{ atoms/m}^2 \cdot \sqrt{2\pi mk_B T}}{Pa_s} \quad t_{ML}(1 \cdot 10^{-4} \text{ Pa}) \approx 1 \text{ s} \quad t_{ML}(1 \cdot 10^{-7} \text{ Pa}) \approx 15.5 \text{ min} \quad (4.1)$$

By using a pressure of $1 \cdot 10^{-6}$ mbar it is found that within seconds the surface is completely covered with contaminants. However, at a pressure of $1 \cdot 10^{-9}$ mbar it will take several minutes for the contaminants to completely cover the surface. Typical contaminants include water molecules which might stick to the chamber walls once it is opened. A baking of the UHV chamber is therefore performed after each exposure to atmospheric pressure. Here the chamber is heated to about 100°C in order to evaporate all molecules residing on the inside chamber walls.

The UHV chamber named 'The Coal Chamber' is used in this project. The equipment used in this study mounted on The Coal Chamber, is described in the following section along with the experimental approach.

The sample consists of a single crystal of Iridium cut in the (111) direction. This crystal is placed in a circular hole in the middle of a flat square sample holder made of Tantalum. A K-type thermocouple plug, consisting of chromel and alumel connectors, is mounted to the lower end of the sample holder. Chromel and alumel wires are spot welded to their respective connectors on the plug, and the two wires are connected by spot welding the free ends together. The junction, which has a temperature dependant voltage, touches the backside of the Ir crystal. Hence, the temperature of the sample can be interpreted by measuring the voltage of the thermocouple. A K-type thermocouple measures temperatures in the range of -200 to 1250°C, [24] which covers the

temperatures used for the sample in these experiments.

The Ir crystal is kept in place by spot welding two Tantalum strips across the crystal and thermocouple, on the backside of the sample holder.

Once inside the UHV chamber, the sample resides in a manipulator. From here the sample can be transferred to the STM or annealed by a filament residing in the manipulator.

4.2 STM Imaging and D₂ Dosage

The STM was used to visualize the coverage of hydrogen on the sample surface, and to characterize the sample both during and between experiments. The STM within 'The Coal Chamber' is an Aarhus STM which is described in chapter 3. Two modes can be used during operation. These modes are the constant current and the constant height modes. In the constant current mode, the tip has a dynamic z-distance to the sample in order to keep the tunneling current constant. This means that the tip moves closer to the sample at areas with a low LDOS and further away from the sample at high LDOS. The current is kept constant by a feedback loop, and the change in height is mapped as the data. The tip height is fixed during constant height mode, as opposed to the constant current mode. As the tip scans the surface, the tunneling current changes since the distance to the sample varies. Therefore, the topography of the surface is mapped as the tunneling current. Since no feedback loop is required, and the tip height is fixed, the time required to create an image is lower in constant height mode. However, since no feedback loop is used the tip is much more likely to crash into structures on the surface such as large step edges or scratches. The advantages of the constant current mode include higher image quality, and a lower probability of damaging the tip. This scanning mode is therefore used during the experiments.

4.2.1 STM Calibration

The tip of the STM is moved by the piezoelectric scanner tube, as also mentioned in chapter 3. This process is highly sensitive to temperature fluctuations and chamber conditions. Therefore, calibration is needed in order to correct the sizes of the STM images. The STM is calibrated using images with atomic resolution. Figure 5.1c shows an image of pure graphene on Ir(111) which is used for calibration. The length of ten graphene hexagons were measured in the x- and y-directions, and the calibration parameters were found by correcting the measured value to match the length of ten graphene hexagons which was found in the literature. The following calibration parameters were found:

$$X : 1.000, \quad Y : 1.033 \quad (4.2)$$

These calibration parameters were used for all STM images shown in chapter 5. A single calibration used for all images should be acceptable, since all the STM images were gathered within the same chamber baking.

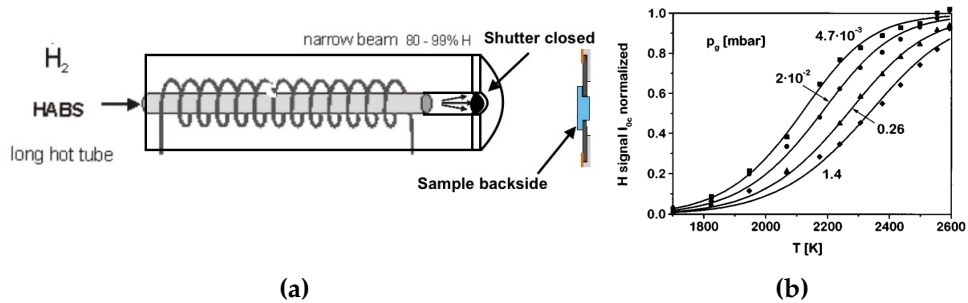


Figure 4.1: (a) Graphic interpretation of the HABS. [25] (b) Hydrogen signal from the HABS as a function of T. [27]

4.2.2 D₂ Dosage

As described in chapter 2, the production of atomic hydrogen is a necessity in order to achieve highly vibrationally excited atoms. Therefore, a hydrogen atom beam source was used (hereafter 'the doser'), in order to dissociate D₂ molecules. The doser consists of a tungsten capillary capable of reaching temperatures up to 2100°C. [25] The capillary is heated by a tungsten filament surrounding the outside, as seen in Figure 4.1a. The temperature of the doser is measured with an integrated C-type thermocouple. This type of thermocouple measures temperatures in the range of 0 to 2320°C, [26] which is needed since the doser has a operating temperature up to 2100°C. [25] A distribution of the flux of atomic hydrogen from the doser as a function of temperature is seen in Figure 4.1b

Each time the graphene on Ir(111) sample was dosed with excited molecules, the sample faced away from the doser. Furthermore, the built in shutter of the doser was closed. This setup is seen in Figure 4.1a. By doing so, no atomic hydrogen reached the sample surface. During dosages of vibrationally excited molecules the ion gauge was turned off. The ion gauge ionizes the molecules within the chamber resulting in a dissociative attachment process once D₂ receives an electron. This results in the formation of atomic hydrogen. [10] Therefore, both the ion gauge and the hot doser are sources of atomic hydrogen, hence the ion gauge had to be switched off during dosing. The pressure in the chamber could not be measured during dosing, and therefore the chamber pressure was estimated from the feeding pressure. This is the D₂ pressure in the gasline during exposure. A pirani gauge was attached to the gasline between the hydrogen source and the doser. The feeding pressure and the chamber pressure were measured at the same time, in order to convert the feeding pressure to a chamber pressure once the ion gauge was turned off. The aim was a chamber pressure of 5 · 10⁻⁷ mbar. The measurement gave the following pressures:

$$\text{chamber pressure : } 5.11 \cdot 10^{-7} \text{ mbar} \quad \text{pirani pressure : } 6.7 \cdot 10^{-2} \text{ mbar} \quad (4.3)$$

During the hydrogenation of graphene on Ir(111) with atomic hydrogen, the sample surface was positioned in front of the tungsten capillary with an open shutter. The ion gauge was turned on during these dosings, since the aim was to obtain a completely hydrogenated graphene on Ir(111) surface.

4.2.3 Sample Annealing and Graphene Repair

The surface of the sample is kept clean by annealing to high temperatures by the filament in the manipulator. This ensures that contaminants on the surface are removed in order to raise the quality of the STM images. After each dose of D₂ the sample was scanned with the STM. Hereafter the hydrogen adsorbed on the surface was removed by heating the sample to above 900 K. After cleaning the surface the graphene was checked in order to ensure that the number of defects was at a minimum. The sizes and shapes of these defects are discussed in chapter 5

If too many carbon vacancies were present, the graphene on the sample was repaired by chemical vapour deposition (CVD). The sample was heated to above 900°C in an ethylene pressure in the range of $1 \cdot 10^{-6}$ mbar. CVD growth of graphene is possible at temperatures above 1120 K, and the structural quality increases with the temperature. [28] During CVD the temperature of the sample surface was measured by an optical pyrometer, since the thermocouple measures the temperature on the backside of the Ir crystal. It is crucial that the Ir(111) surface is at least 1120 K in order to break the ethylene bonds on the Ir(111) surface.

As a further study of the dissociation of hydrogen on graphene, bilayered graphene was grown on the Ir(111) surface. This was done in accordance with the CVD procedure explained above. However, the sample was annealed for a long time (1-2 hours) during the growth of bilayers.

4.3 TPD

A quadrupole mass analyser is connected to the UHV chamber, which was used to investigate the desorption of deuterium from the sample surface. The sample was positioned in the manipulator and heated with the filament as the experiments were carried out. From here the nozzle of the mass spec was brought within a millimeter of the sample. The temperature of the sample was logged together with the amount of desorbed deuterium detected by the quadrupole. The mass spec was set to count masses of 4 amu, in order to exclude other molecules than deuterium.

A Eurotherm 2704 controller was used to control the temperature of the sample by altering the current running through the filament in the manipulator. The controller was programmed to ramp the sample temperature from 300 K to 900 K at a rate of 1 K per second. At maximum temperature the eurotherm was set to rest for 30 s, and then slowly decrease current as the temperature dropped to a final temperature of 300 K. This cycle was performed each time a TPD measurement was carried out. After this procedure all of the deuterium on the surface is desorbed from the sample. As mentioned the temperature measured by the thermocouple is only valid for the backside of the sample. Therefore a calibration of the system is needed in order to find the correct peak temperatures. A calibration was done where the sample surface was measured with an optical pyrometer along with the thermocouple temperatures. Both temperatures were logged each time the temperature rose 30°C. The results from this calibration are seen in Figure 4.2. It is seen that there is no linear temperature ramp until the thermocouple reading is around 600 K. This is due to the limitations of the pyrometer. The pyrometer measures the emitted radiation from a solid object, and in order to get a reading, the intensity of the emitted light from the measured object must be significant. [29] However, a fit was made from the data points with a linear tendency. The

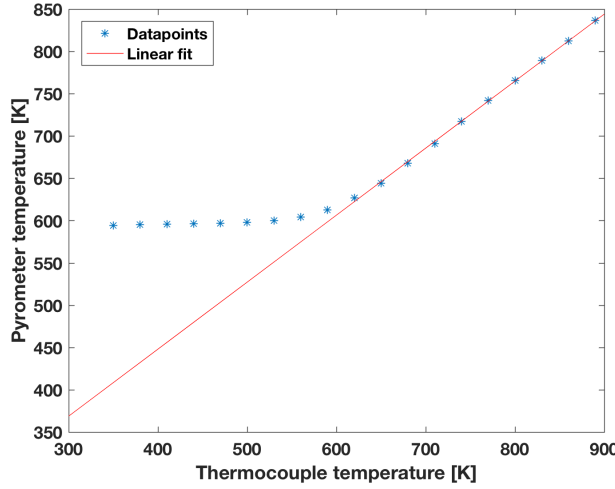


Figure 4.2: Calibration of the temperature during the TPD measurements. The temperature of the surface measured by an optical pyrometer is plotted against the thermocouple temperature.

fitted line had the following parameters:

$$T_{surface} = T_{TC} * 0.7921 + 131.2K$$

In Figure 4.3a the data obtained from a typical TPD measurement is shown. Since the desorption of D₂ from the surface is investigated, a mass of 4 amu is monitored along with the temperature of the sample. It is seen that the temperature follows a linear ramp. Some fluctuations are however seen in the beginning and end of the temperature interval.

TPD measurements were conducted on a new sample with a different sample holder and a new thermocouple. Therefore, the Eurotherm controller parameters needed to be autotuned, in order to achieve a linear temperature ramp once again. This autotuning was unsuccessful, and the results from one of the TPD measurements from this sample can be seen in figure 4.4. It is seen in Figure 4.4a that the temperature ramp is far from linear. The jumps in temperature do not seem to be systematic, which might indicate that the thermocouple as well as the controller parameters both had influence on the bad temperature ramp. The influence of the non linear ramp is also seen on the D₂ counts, where small peaks appear when the temperature changes rapidly. As seen in Figure 4.4b another peak appears right after the initial peak due to the jump in temperature. However, it is seen that the D₂ counts were descending prior to the second peak, and therefore the initial peak was judged to fit the desorption of hydrogen best. It was not possible to conduct new TPD measurements due to time limitations.

The peak temperatures are needed in order to calculate the desorption energies from the Redhead method. Peak temperatures were found by fitting a triple gaussian function to the data points. The peak temperature was initially estimated by visual observation, and the data points within $\pm 60^{\circ}\text{C}$ of this guess were included in the fit. It is seen in Figures 4.3b and 4.4b that a triple gaussian function has a good fit to the data points. Using this function should be acceptable since the peak temperature is the only wanted quantity. The green circle in figure 4.3b shows the found peak

from which the sample temperature was gathered. These temperatures are found for each TPD measurement and all of these are presented in chapter 5. The desorption energy is estimated by the Redhead method described in chapter 2.

In order to compare the individual peaks, the background was subtracted from every data point. The sample was positioned stationarily in front of the nozzle, and data was acquired for a period of time before each temperature ramp was started. These data points prior to the temperature ramp were used to calculate a mean background count, which was subtracted.

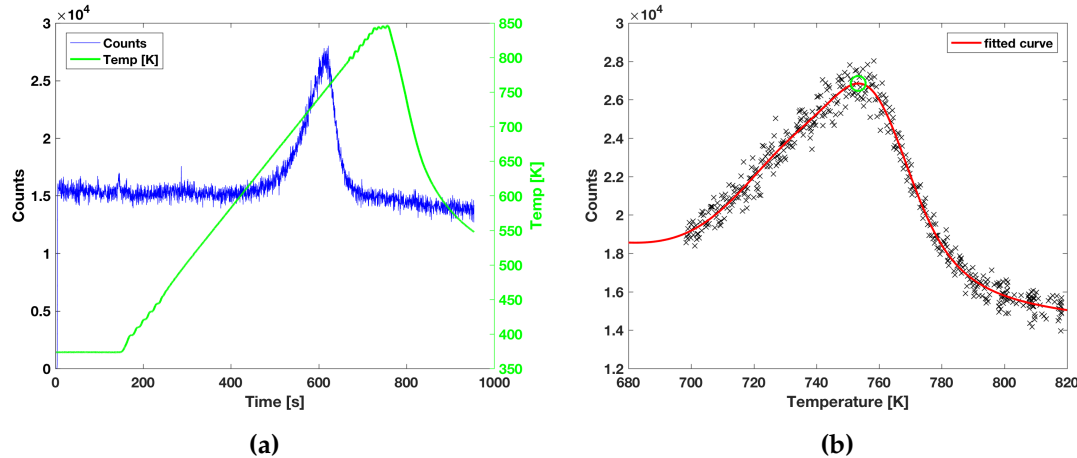


Figure 4.3: example of TPD measurements from the main sample. (a) shows data acquired from the quadrupole mass analyser and thermocouple readings. (b) shows the curve fitted to the data points within $\pm 60^\circ\text{C}$ of the estimated peak value.

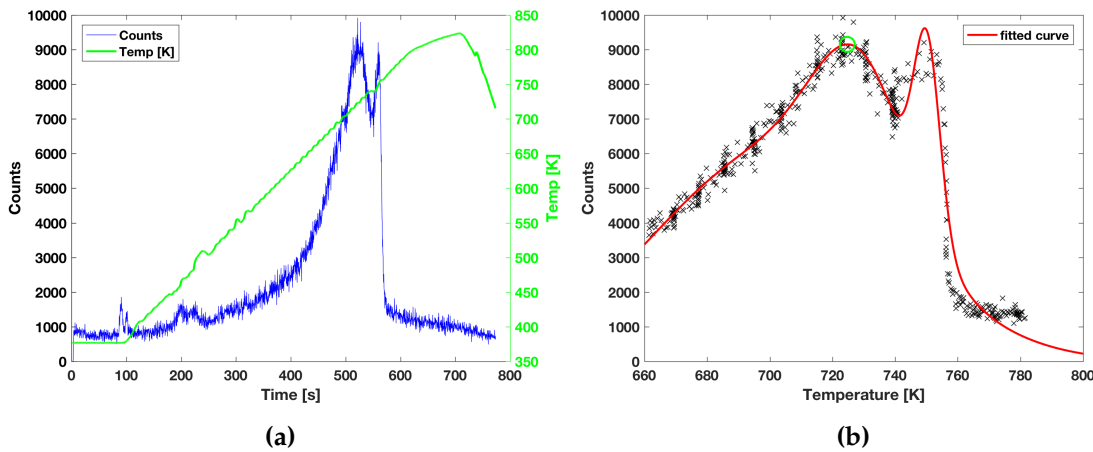


Figure 4.4: example of TPD measurements from the new sample. (a) shows data acquired from the quadrupole mass analyser and thermocouple readings. (b) shows the curve fitted to the data points within $\pm 60^\circ\text{C}$ of the estimated peak value.

5

Results

The techniques and procedures presented in the preceding chapters are all used to study an Ir(111) crystal with a graphene monolayer on top. In the following section STM images of pure graphene on Ir(111) are presented. This graphene was grown prior to these experiments by CVD.

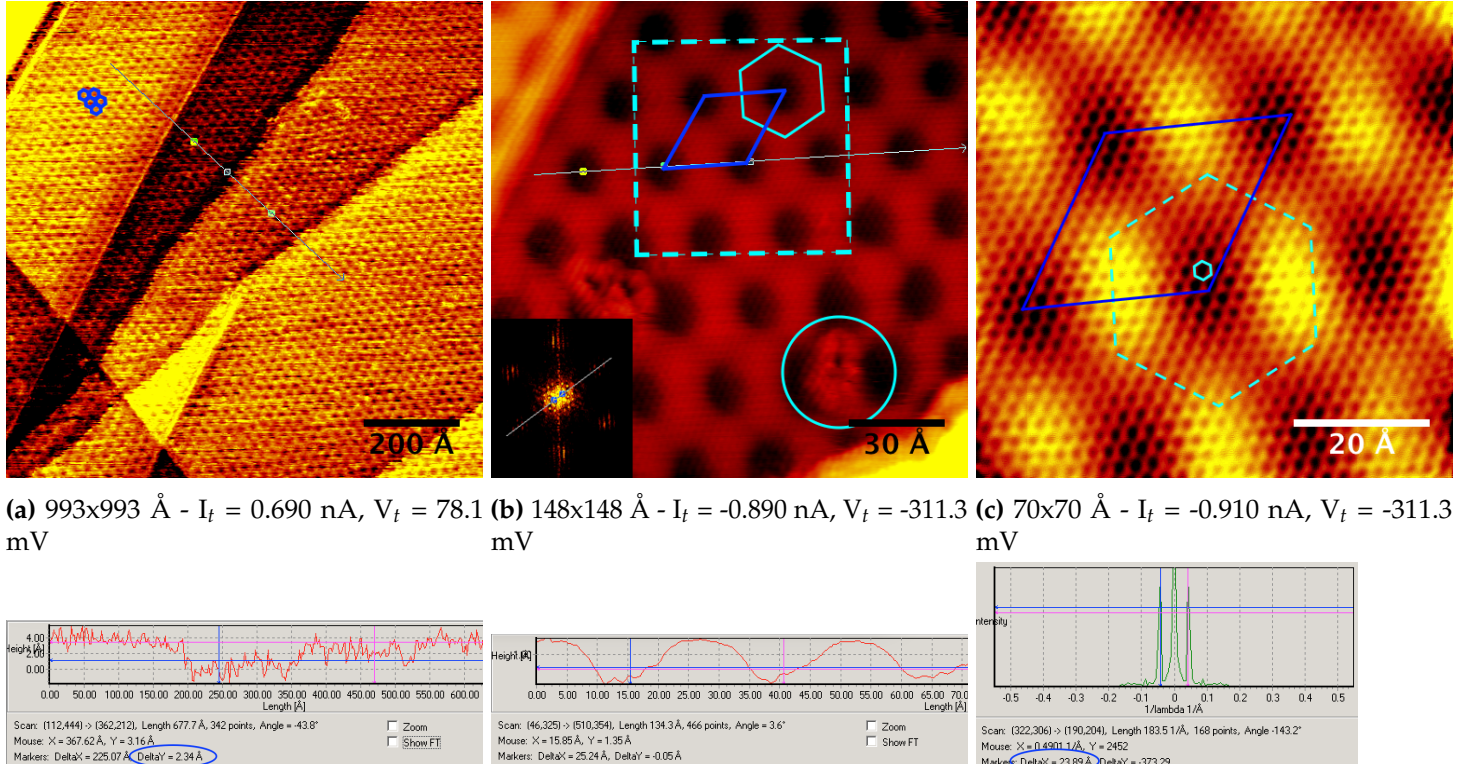
5.1 Graphene on Ir(111)

STM images of pure graphene on Ir(111) are shown in this section. Figure 5.1 shows images of graphene on Ir(111) on different scales and, Figure 5.1a shows a large image of a graphene monolayer covering the Ir(111) surface. Although the quality of the image is poor, which is seen as lines dragged across the surface, the moire pattern can be perceived as a pattern of small hexagonal structures. The blurred lines can be caused by the tip picking up an atom which momentarily changes the LDOS of the tip until the atom is dropped on the surface once again. The hexagonal structures caused by the moiré pattern, are outlined in the top left of the image. Some step edges from the underlying Ir surface are also seen. A line scan of one of these has been performed, which shows that the height difference is $2.34 \pm 0.4 \text{ \AA}$. This value is consistent with the value of 0.22nm found in the literature. [28,30]

An image displaying a closer look of Graphene on Ir(111) is seen in Figure 5.1b. The moire pattern is very prominent in this figure, which once again is outlined as the blue hexagon. A moiré unit cell is also sketched as a blue rhombus, and the spacing between the individual sites in the moiré unit cell can be determined from a line scan. A line scan was drawn in Figure 5.1b, and two points were positioned in the ATOP sites of the graphene on Ir(111) in order to obtain the moire periodicity. The moiré periodicity is $25.2 \pm 0.4 \text{ \AA}$ according to the literature. [5] This agrees with the length of $25.24 \pm 1 \text{ \AA}$ measured from the line scan, which is seen in Figure 5.1e. A fast fourier transform was mode from the picture which is shown as the inset in Figure 5.1b. By measuring between two of the intensity peaks a mean value of the moiré periodicity on the entire image is found. This value is measured to $23.89 \pm 1 \text{ \AA}$ which is seen in Figure 5.1f. Typical defects of the graphene monolayer are seen in this figure, within the blue circle. These defects are probably caused by carbon vacancies.

Figure 5.1c shows a high quality image of the graphene monolayer on top of Ir(111). This image is a zoom in of the image shown in Figure 5.1b corresponding to the dashed square. The hexagonal

pattern is the graphene monolayer on top of the iridium. The graphene hexagon is sketched as the full blue hexagon and the moiré pattern seen on the two preceding figures is sketched as the dashed blue hexagon. The moiré unit cell is shown in the form of the blue rhombus, where the four dark corners correspond to the ATOP sites. The HCP and FCC sites lie at the corners of the dashed blue hexagon within the outlined moiré unit cell.



(d) Line profile of the line scan in Figure (a) (e) Line profile of the line scan in Figure (b). (f) Line profile of the FFT scan in Figure (b).

Figure 5.1: Clean graphene on Ir(111). (c) is a zoom in of (b) which is shown as the dashed square.

5.2 D₂ on Graphene

The following sections present the data obtained following exposure of the sample to vibrationally excited molecules. The experiments aimed at determining the threshold temperature of the doser, where very few vibrationally excited molecules are produced. Hence, the temperature of the doser was varied in order to alter the flux of atoms from the doser, and thereby changing the number of hydrogen recombinations on the walls within the chamber as described in chapter 2. Therefore, the data include D₂ exposure at doser temperatures of 1343°C, 1543°C, and 1745°C. The dosage time and D₂ pressure were identical in all of these doses, in order to ensure that the doser temperature was the only variable changed. A dose at 1300°C was also performed. However, the STM broke, and therefore we did not get any images. Furthermore images are included from a fully hydrogenated graphene on Ir(111) surface. These images were compared to images of the short dosage experiments and they are presented first.

5.2.1 Full Hydrogen Coverage

The fully hydrogenated surface was made by filling the chamber with hydrogen at a pirani pressure of $6.8 \cdot 10^{-2}$ mbar. This pressure should correspond to a chamber pressure of $5 \cdot 10^{-7}$ mbar, according to the calibration mentioned in chapter 4. The ion gauge was turned off during the dosing, in order to imitate the chamber conditions at short dosage periods. The dosage time was 60min.

Figure 5.2 displays images of different scales. As seen from Figure 5.2a, the sample is fully hydrogenated even at relative large areas of 992x992 Å. Ring structures cover the surface of this image, instead of the moiré pattern observed in Figure 5.1a. These structures can be more easily seen in Figure 5.2b, which is a zoom in of Figure 5.2a. The hydrogenated surface most often shows ring shaped patterns in the form of structures with a bright rim and a darker center. By comparing Figures 5.2b and 5.1b it is obvious that the adsorption of hydrogen on the surface changes the LDOS. It is noticeable that the defects seen in Figure 5.1b resemble the ring shaped structures seen in Figure 5.2. Consequently, these defects might be caused by adsorbed hydrogen. Furthermore, some H-structures on the saturated surface seem to merge into a bigger structure, seen as the three point star shaped structures marked with arrows in Figure 5.2b. A FFT was made in order to check the periodicity of the pattern on the hydrogenated surface which is seen as the inset in Figure 5.2c. The related profile is shown in Figure 5.2d, and although the surface is much less periodic, some periodic structures are found with 21.79 ± 1 Å. This value is very close to the periodicity of the moiré unit cell. This result is expected since it is known that hydrogenation happens at the specific sites in the moiré unit cell as mentioned in chapter 2.

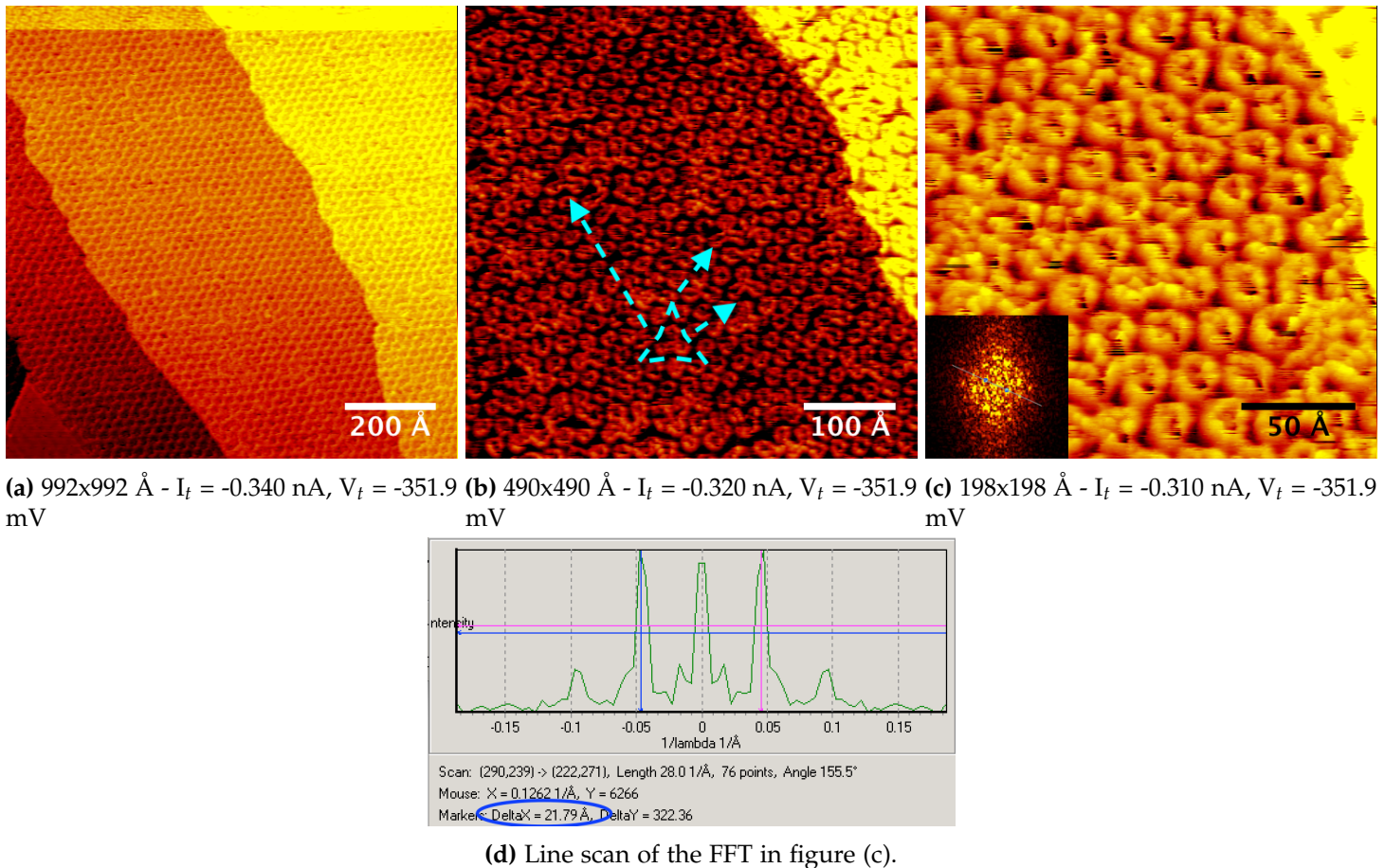
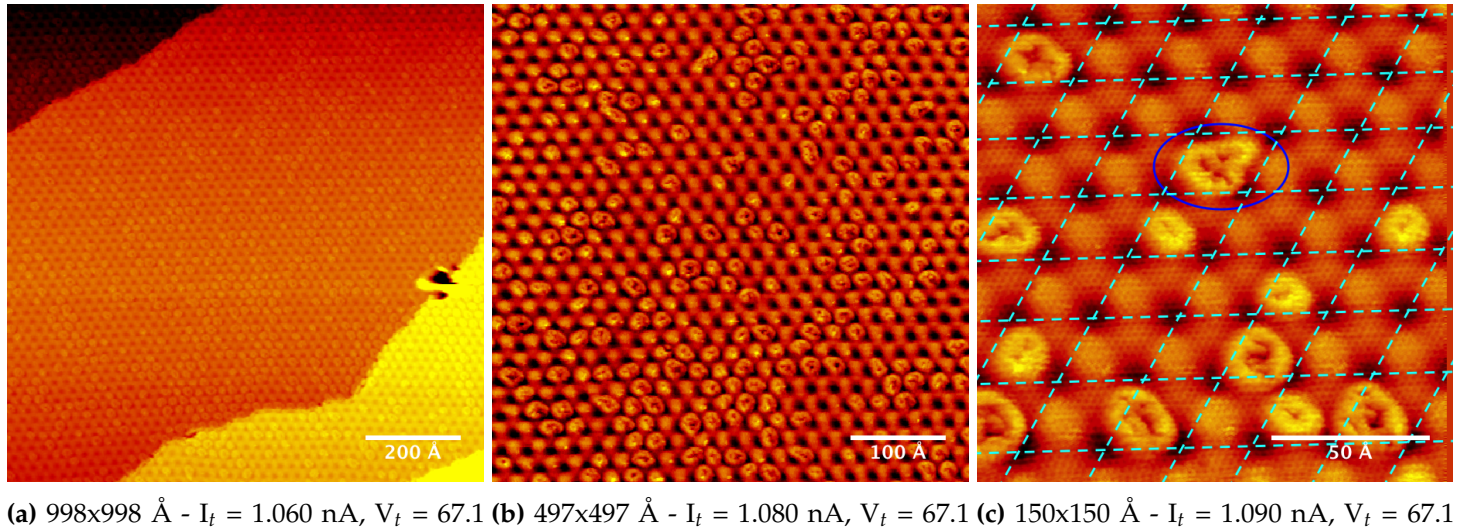


Figure 5.2: Fully hydrogenated Gr/Ir(111) surface after 12h D₂ dosage. (c) is a zoom in on (b)

5.2.2 1745°C Dose

This dosing was performed at a pirani pressure of $6.8 \cdot 10^{-2}$ mbar, and with the doser set at a temperature of 1745°C. The dosage time was 20 min. The graphene was checked before dosing in order to reduce the number of defects as much as possible. Three images at different scales are shown in Figure 5.3. These images were taken immediately following the completion of the dosing. Comparing Figures 5.3a and 5.2a, the surface in Figure 5.3a is far from saturated, since the moiré pattern can be observed between areas in which the distinct ring structure of the hydrogenation is seen. It is also interesting that none of the hydrogenated sites melts together to form bigger structures, which indicates that this phenomenon happens as the surface becomes saturated. In Figure 5.3 each moiré unit cell has been sketched with blue dashed lines. This shows that hydrogenation only happens at one site in the bottom left corner of the moiré unit cell. Earlier studies suggest that this is the FCC site in the moiré unit cell. [31] It is, however, seen that in some of the unit cells hydrogenation expands to the HCP site. This is illustrated by the dark blue circle. Individual hydrogen atoms are not distinguishable in the STM images, and therefore the coverage is estimated as a percentage of the number of hydrogenated moiré unit cells to the total number of moiré unit cells. Figures 5.3b and 5.3c were used to estimate the extent of hydrogenation of

the surface. The fraction in Figure 5.3b was calculated to 41% and the fraction in Figure 5.3c was calculated to 29%. This means that about one third of the unit cells is hydrogenated after a dosage of excited molecules for 20 min, at a chamber pressure of $5 \cdot 10^{-7}$ mbar.



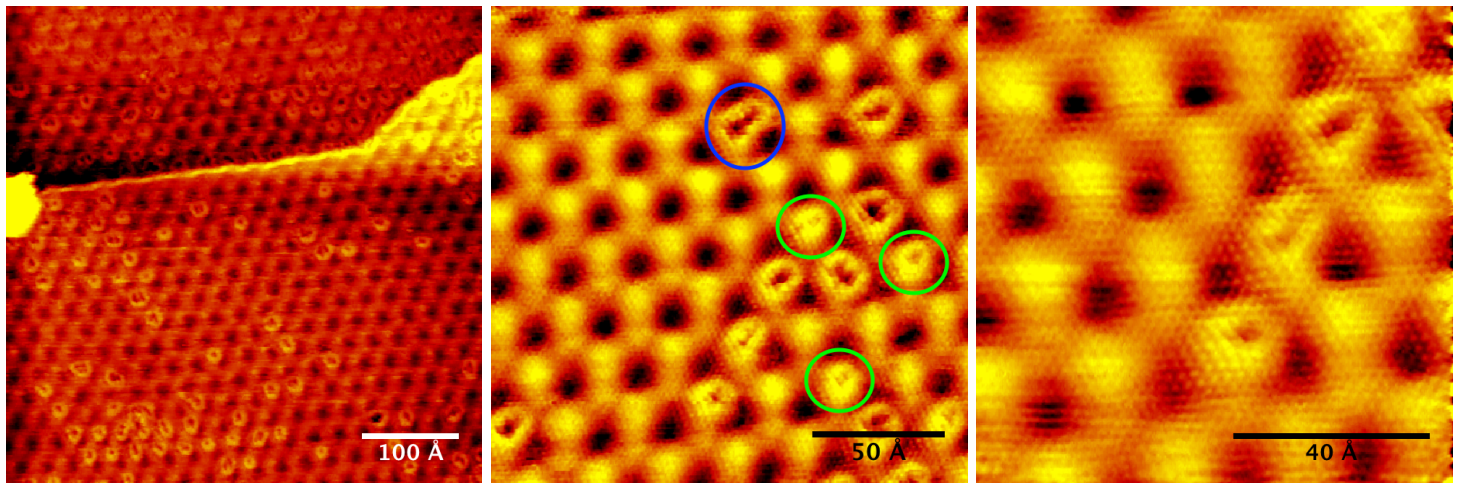
(a) 998x998 Å - $I_t = 1.060$ nA, $V_t = 67.1$ mV (b) 497x497 Å - $I_t = 1.080$ nA, $V_t = 67.1$ mV (c) 150x150 Å - $I_t = 1.090$ nA, $V_t = 67.1$ mV

Figure 5.3: Hydrogenated Gr/Ir surface after dose of D₂ at a doser temperature of 1745°C.

5.2.3 1593°C Dose

This dosing was performed at a pirani pressure of $6.8 \cdot 10^{-2}$ mbar and a doser temperature of 1593°C. Again the dosing lasted 20 min. The images obtained after the dosing are shown in Figure 5.4. There is a remarkable resemblance between the pictures shown in Figures 5.3 and 5.4. Again, both the ring shaped structure itself, and its shape are very similar to the ones observed earlier. Several ring structures are seen along the Ir step edge in Figure 5.4b. The energy barrier is known to be less at step edges and dislocations [12], hence molecules excited to lower vibrational states might be able to hydrogenate the graphene in these regions. This could explain the hydrogenation along the step edge.

Some of hydrogenated sites In Figure 5.4b seem to stretch beyond the FFC site as well. One of these is marked with a blue circle. Furthermore some of the ring shaped structures, marked with green circles, seem smaller compared to those observed earlier. As mentioned, recent DFT calculations have shown that the initial barrier perceived by a hydrogen molecule is 3 eV, which then is reduced to 2 eV after dissociation of the first molecule. [12] Therefore it is only the highest vibrational states that contain enough energy to dissociate. These smaller ring structures might therefore only contain a few hydrogen atoms, and are therefore probably emerged right before dosing stopped. Figures 5.4a and 5.4b were used to calculate the fraction of hydrogenated moiré super cells, with values of 32% and 25%, respectively.



(a) 488x488 Å - $I_t = 0.900$ nA, $V_t = 190.4$ mV
(b) 180x180 Å - $I_t = 1.020$ nA, $V_t = 190.4$ mV
(c) 97x97 Å - $I_t = 1.020$ nA, $V_t = 190.4$ mV

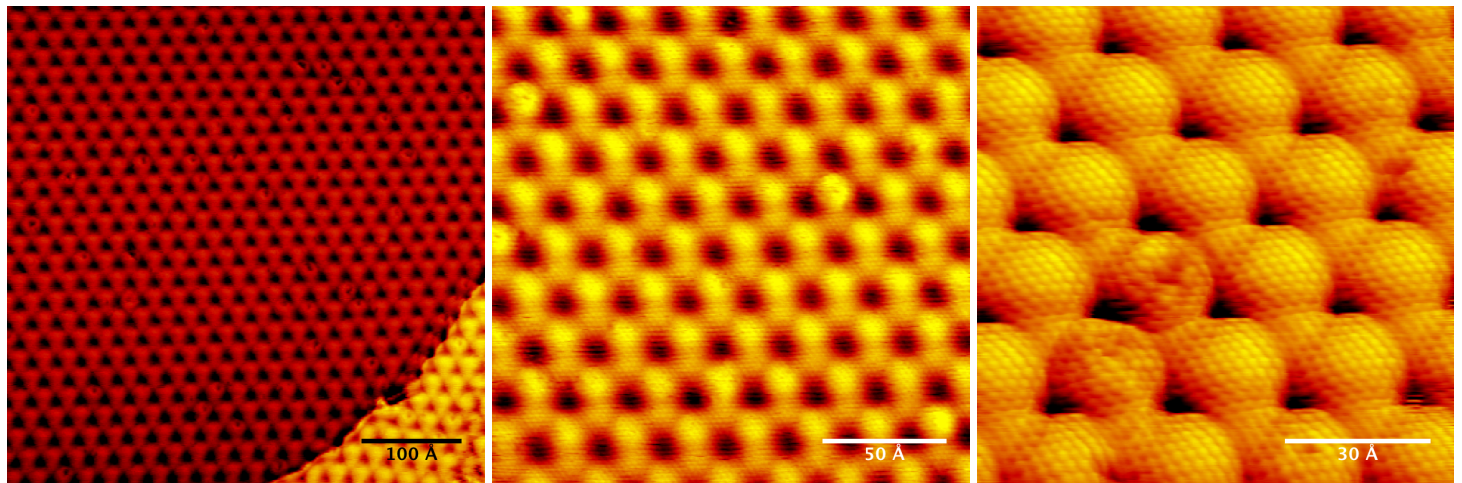
Figure 5.4: Hydrogenated Gr/Ir surface after dose of D₂ at a doser temperature of 1593°C.

5.2.4 1343°C Dose

The pirani pressure was measured to $6.8 \cdot 10^{-2}$ mbar, and the doser had a temperature of 1343°C during this dosing. Hydrogen was dosed for 20 min. As seen in Figure 5.5 several high quality pictures of the sample were taken. In Figure 5.5a the observation of several ring shaped structures indicates that some hydrogen is adsorbed. As a zoom in is made such as the one in figure 5.5b the defects differ from those seen earlier in Figures 5.4b and 5.3c. The ring shaped structures are much smaller in diameter in Figure 5.5b, even though the scanning parameters are close to each other. A high resolution image is seen in Figure 5.5c, where the hexagonal graphene is highly visible. In this image it is clear that the graphene is defected, although it is unclear whether this is due to the presence of hydrogen. It should be noted that the graphene had defects before the dose was initiated. The abundance of these defects was indistinguishable, when comparing before and after the dose. Therefore it is not possible to conclude whether the threshold temperature of the hydrogen adsorption from excited molecules lies at 1340°C. It is however very likely that no hydrogen is adsorbed since these defects resemble carbon vacancies as seen in the litterature. [28]

In order to investigate the threshold temperature further, it would be rational to conduct TPD measurements of the sample after hydrogen dosage at 1343°C. This experiment would determine whether any hydrogen is adsorbed on the graphene.

It is also seen that the shape of the sites in the moiré unit cell has changed although both pictures are from the same scan session. This is due to a tip effect, where the LDOS of the tip has probably changed, which affects the tunnelling current. This might happen if the tip picks up an atom from the surface, or if the physical dimensions of the tip changes after a tip treatment.



(a) $477 \times 477 \text{ \AA}$ - $I_t = 0.820 \text{ nA}$, $V_t = 20.1 \text{ mV}$ (b) $192 \times 192 \text{ \AA}$ - $I_t = 0.830 \text{ nA}$, $V_t = 55.8 \text{ mV}$ (c) $98 \times 98 \text{ \AA}$ - $I_t = 0.820 \text{ nA}$, $V_t = 20.1 \text{ mV}$

Figure 5.5: Hydrogenated Gr/Ir surface after dose of D_2 at a doser temperature of 1343°C .

5.3 TPD measurements

The following sections compare TPD measurements from graphene on Ir(111) exposed to vibrationally excited molecules and atomic hydrogen.

5.3.1 Atomic and molecular D_2 - single layered sample

In Figure 5.6 below, the data from the TPD is gathered in two different figures. TPD measurements were made following doses of vibrationally excited molecules and atomic hydrogen on the new sample with a fresh monolayer of graphene on Ir(111). Figure 5.6a shows the TPD data following a 60 min dosing of D_2 at a chamber pressure of $5 \cdot 10^{-7} \text{ mbar}$ and a doser temperature of 1740°C . The data in Figure 5.6b is from a 60 min dosing of hydrogen atoms at a chamber pressure of $5 \cdot 10^{-7} \text{ mbar}$ and a doser temperature of 1740°C .

A single peak is observed after dosing excited molecules which is seen in Figure 5.6a. A big peak is seen after the main peak, at a temperature of about 800 K. This is due to a temperature spike caused by the Eurotherm temperature controller, which was poorly calibrated as explained in chapter 4. Noticeable fluctuations caused by this problem are also seen in Figure 5.6b. This dataset was gathered when applying the same chamber and sample conditions as the blue graph in Figure 5.6a.

The temperature at the peak was found by the procedure described in chapter 4. The single peak in Figure 5.6a must correspond to the hydrogen adsorbed on the HCP and FCC sites in the moiré unit cell. This peak was present in all TPD data sets and the temperatures of these are shown in Table 5.1. The calculated energies of desorption by the Redhead method are all around 2 eV. This value is close to the calculated average hydrogen binding energy of 2.20 eV [32] within a graphane like island. Also DFT calculations done by Mie Andersen have shown that the dissociative desorption energy of hydrogen is 2.12-2.25eV, [33] which again is in agreement with the calculated values in

| Sample | fig.5.6a blue | fig.5.8a green | fig.5.6b blue | fig.5.8b green | fig.5.7 green | fig.5.7 red |
|--------------------------|---------------|----------------|---------------|----------------|---------------|---------------|
| Peak T [K] | 724.8 | 698.4 | 694.0 | 709.1 | 739.1 | 753.4 |
| $E_{des}^{Redhead}$ [eV] | 2.1 ± 0.4 | 2.0 ± 0.4 | 2.0 ± 0.4 | 2.0 ± 0.4 | 2.1 ± 0.4 | 2.1 ± 0.4 |

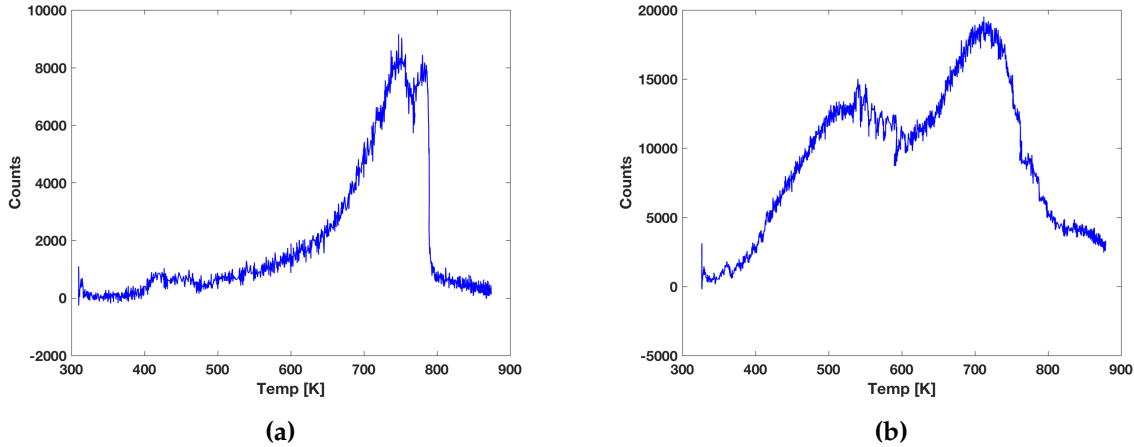
Table 5.1

Figure 5.6: TPD measurements following doses of D₂ and atomic hydrogen. (a) shows the graph following a 1 hour D₂ dose on graphene on Ir(111) with a doser temperature of 1740°C and a chamber pressure of $5 \cdot 10^{-7}$ mbar. and (b) shows the graph following a 1 hour D dose on graphene on Ir(111) with a doser temperature of 1740°C and a chamber pressure of $5 \cdot 10^{-7}$ mbar.

this thesis. As mentioned recent research has shown that the initial hydrogen molecule perceives an adsorption barrier of 3 eV. Hereafter the adsorption barrier undergoes a reduction of 1 eV due to the distortion of the graphene from the sp² to sp³ rehybridization. [12] Compared to this the energy of desorption calculated by the Redhead method seem reasonable.

Another peak appears when observing the data after the dosing with atomic hydrogen, as seen in Figure 5.6b. Hydrogen desorbs from the sample at two different desorption energies, which is seen from the two peaks. The temperature of these peaks were found by the same procedures as earlier, and the values were found to be 550.4K and 694.0 K. The lower peak suggests that a different type of Gr-H bond is present. The most plausible explanation is the presence of hydrogen dimers on the ATOP site of the moiré unit cell. The presence of these are supported by the litterature, with DFT calculations. [32] Earlier TPD measurements of deuterium dosed on highly ordered pyrolytic graphite (HOPG) have shown that dimer peaks appear at 445K and 560 K. [34] These values are in correspondence with the peak in Figure 5.6b. However, through discussions with the lab supervisor it was suggested that the peak intensity in this figure is too high to stem from dimers. Therefore hydrogen must desorb from another source within the chamber during the TPD measurements. It is reasonable that this contribution come from the desorption of hydrogen from the Tantalum sample holder.

5.4 Graphene bilayered sample

As a further study of the adsorption of hydrogen on Gr/Ir, patches of graphene bilayers were grown on the sample by annealing in ethylene for long periods of time. The sample was investigated with several techniques, and the results are presented in the following sections.

5.4.1 TPD of bilayered sample

TPD measurements were conducted on the sample before and after an anneal in ethylene for 60 min. The red graph in figure 5.7 is the TPD results following the 60 min dose of D₂ at a chamber pressure of $1.04 \cdot 10^{-6}$ mbar and with a doser temperature of 1740°C.

The green graph corresponds to the sample after bilayers supposedly were grown. Bilayers were grown by exposing the sample to ethylene at a pressure of $1 \cdot 10^{-6}$ mbar for 60 min, while the sample was heated to 990°C. The sample was dosed with atomic hydrogen at a chamber pressure of $1.04 \cdot 10^{-6}$ mbar and with a doser temperature of 1740°C as well as before. It is seen that the peak value this time is around 6.000, which means that the increased amount of bilayers reduce the amount of hydrogen on the surface by a significant amount. This suggests that hydrogen is not adsorbed on the bilayered graphene. This theory is supported by the STM pictures below.

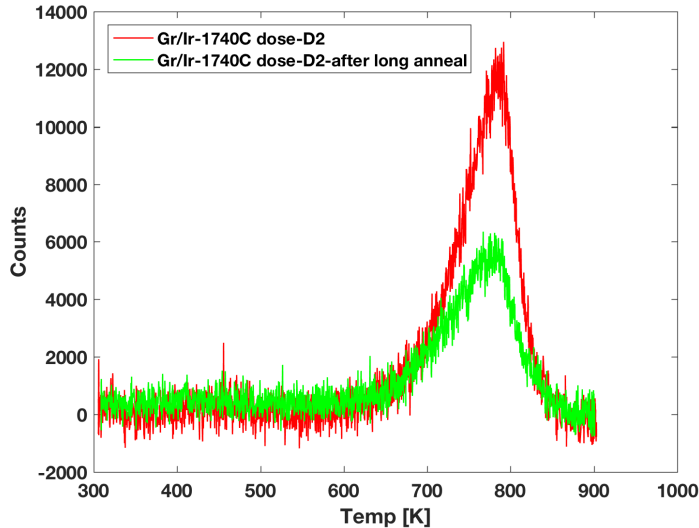


Figure 5.7: TPD measurements after doses of D₂ at a pressure of $1.04 \cdot 10^{-6}$ and a doser T of 1740°C. The red graph is prior to a 60 min growth of bilayers where the 990°C sample was exposed to ethylene for 60 min at a pressure of $1 \cdot 10^{-6}$ mbar

TPD measurements following doses of D₂ and atomic hydrogen, were also conducted on the bilayered sample. These measurements were conducted on the sample as previous, following another anneal in ethylene for 2 hours at a pressure of $1 \cdot 10^{-6}$ mbar. The Eurotherm was calibrated nicely during these experiments, and hence a smooth linear ramp of 1K/s were used. Figure 5.8a shows the graph following a 1 hour D₂ dose on graphene on Ir(111) with a doser temperature of

1740 °C and a chamber pressure of $5 \cdot 10^{-7}$ mbar. Figure 5.8b shows the graph following a 1 hour D₂ dose on graphene on Ir(111) with a doser temperature of 1740°C and a chamber pressure of $5 \cdot 10^{-7}$ mbar. Only a single peak

As seen in Figure 5.8a a single peak is observed following the dose with vibrationally excited molecules. However, as the sample is dosed with atomic hydrogen, a small peak seem to appear between 400 K and 600 K. This peak should correspond to the dimer structures in the ATOP sites of the graphene. In contradiction to the peak observed in Figure 5.6b, this peak is a lot smaller. This might indicate that the nozzle of the quadrupole was closer to the sample during the TPD. Comparing Figures 5.8a and 5.8b it is furthermore observed that the peak at 700 K has a higher value in Figure 5.8b. This might be due to hydrogen adsorbed on the bilayered graphene.

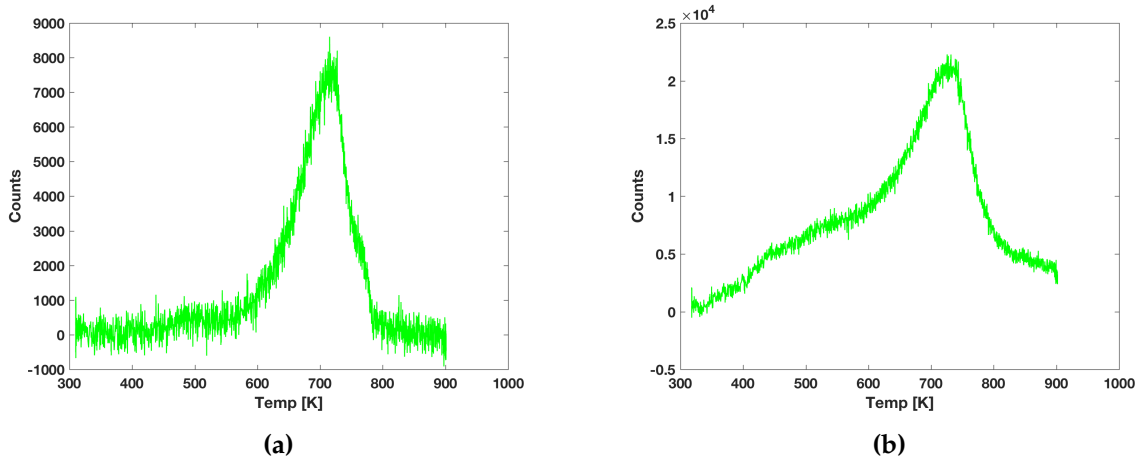


Figure 5.8: TPD measurements following doses of D₂ and atomic hydrogen. (a) shows the graph following a 1 hour D₂ dose on graphene on Ir(111) with a doser temperature of 1740°C and a chamber pressure of $5 \cdot 10^{-7}$ mbar. and (b) shows the graph following a 1 hour D dose on graphene on Ir(111) with a doser temperature of 1740°C and a chamber pressure of $5 \cdot 10^{-7}$ mbar.

5.4.2 STM images of bilayers

In the following section STM images of bilayer patches are included. These images are made prior to the long anneal, and are therefore not directly related to the experiment mentioned in the preceding section. It was not possible to make images of the sample after the long anneal in ethylene, since the STM was broken. Bilayers were however present on the surface prior to the long anneal, and the following images show some of the key points about these.

In Figure 5.9a an image following a 60 min D₂ dose at a pressure of $5 \cdot 10^{-7}$ mbar is included. From this image it is obvious that no adsorption of hydrogen happens on bilayer patches. This is seen due to the change in pattern in the bilayer patch and the surrounding surface. A very close look on the image reveals the graphene pattern. The moiré structure from the Ir(111) surface is furthermore preserved. This is different on the images described below.

The images in Figures 5.9b and 5.9c are made after a 12 hour dose of hydrogen at a chamber pressure of $1 \cdot 10^{-5}$ mbar with the ion gauge turned on. Hence the surface is fully hydrogenated which is difficult to see due to the large images. In Figure 5.9b, the three-point-star-structures

characteristic for the hydrogenated surface are however seen, which is pointed out with the blue arrows. Bilayer patches are seen on the top half of the figure, and none of the structures characteristic for the fully hydrogenated surface are seen. A new superstructure is however seen with the individual flower-like structures, with a center circle surrounded by six other circles, construct a bigger pattern. This changed pattern might arise due to a mismatch between the two graphene layers.

In Figure 5.9b a line scan was made across the edge of the graphene monolayer-bilayer edge. The corresponding line profile is shown in figure 5.9d, and from this the height difference is measured to $2.97 \pm 0.5 \text{ \AA}$. The bilayer edge is therefore significantly higher than the Iridium step edge, and much closer to the layer height of HOPG which is 0.35nm. [35]

In order to investigate the bilayer superstructure further, a zoom in of Figure 5.9b was made as seen in figure 5.9c. The graphene sheet is seen due to the atomic resolution, and it is obvious that no hydrogen is adsorbed to the surface. This is consistent with the data from the TPD measurements. Furthermore it is seen that the consistency in the superstructure is absent. Some areas of the bilayer has a cluster of three circles forming a triangle that points either up or down. These are highlighted in the left side of the picture. Other areas seem to have the flower-like structure mentioned earlier, but with an overlapping hexagon. An attempt to determine the periodicity of the superstructure was done by doing a linescan between two identical parts of the pattern. As seen In Figure 5.9c the linescan was drawn between two down facing triangles, and the distance between these were measured from the bottom corner. The line profile is shown in figure 5.9e and the length between the points is measured to $45.78 \pm 1 \text{ \AA}$.

5.4.3 LEED of bilayered sample

LEED was performed on the bilayered sample as the last experiment. The figures in 5.10 show pictures of the fluorescent screen within the UHV chamber from which the LEED was performed. The image In Figure 5.10a shows the fluorescent screen after the untreated sample was exposed to an electron beam with an energy of 145 eV. The spots marked out with the marked arrows show the diffraction pattern from the underlying Ir(111) surface, as well as the graphene sheet on top of the surface. [5]

The sample was then flashed to a low temperature in order to maintain any bilayers, and the sample was once again exposed to an electron beam of energy 145 eV. The top and bottom right corner of the hexagonal pattern is enlarged in figure 5.10b. From this figure it is clear that some extra spots appear around the Ir and C spots pointed out in the previous figure. These spots arise from the moiré pattern of the graphene on Ir(111) surface. The reason why these spots were absent in the previous figure might be caused by a high amount of contaminants on the surface. These ruin the periodicity of the surface, and hence also the electron scattering, which then becomes smeared out. After annealing to a low temperature these contaminants should be gone, leaving the surface clean with small patches of bilayered graphene. The patches of bilayered graphene should however also cause a different scattering due to the changed periodicity as seen in figure 5.9c. If figure 5.10b and 5.10c is compared it does look like the spot belonging to the carbon atoms and the surrounding moiré spots in figure 5.10b are less distinct. These results might therefore

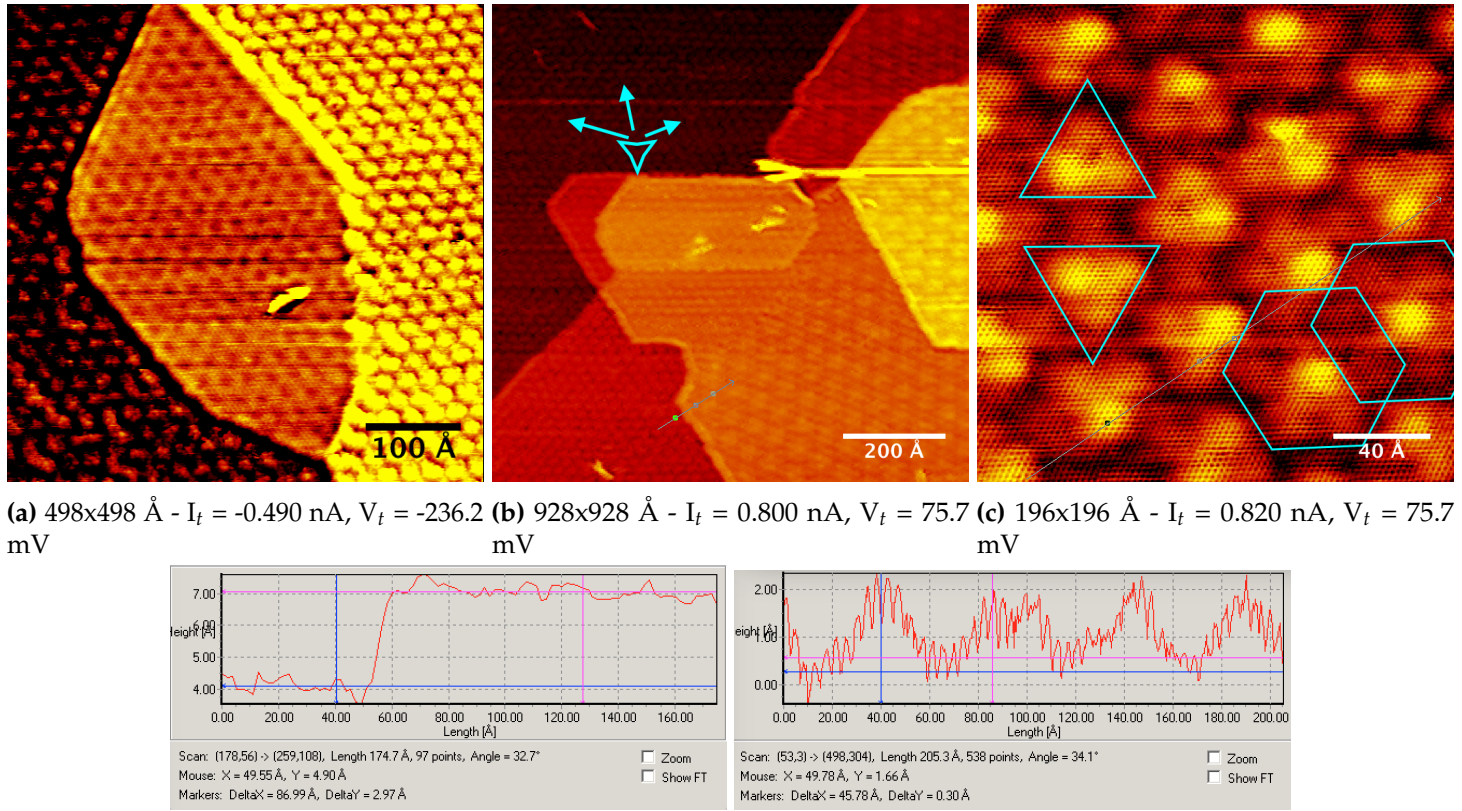


Figure 5.9: Patches of bilayered graphene on Ir after a hydrogen dose at $1 \cdot 10^{-5}$ mbar for 12h.

indicate that bilayers are present on the surface in figure 5.10b and to a lesser extent in figure 5.10c. Since the picture in figure 5.10c is taken after an 1090°C anneal, it is reasonable to conclude that the bilayer patches disappear from the surface when annealing to this temperature.

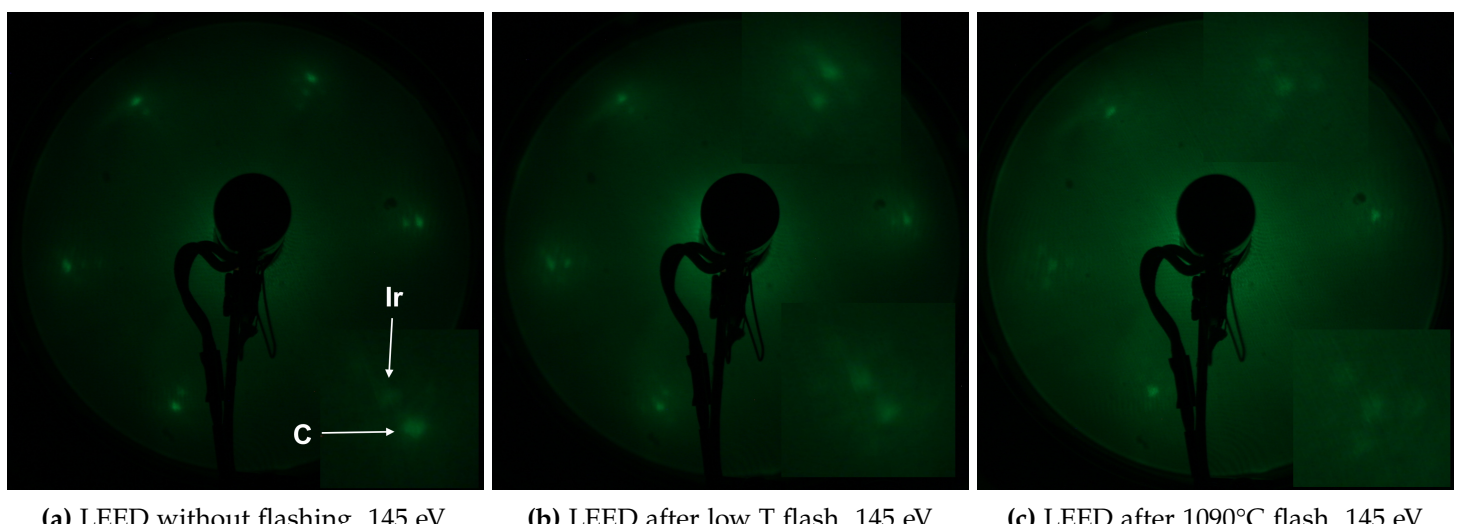


Figure 5.10: LEED pictures from the graphene on Ir(111) sample with bilayers. [36]

Conclusion and Future Perspectives

Pure graphene on Ir(111) was initially investigated along with the defects by carbon vacancies. The moiré pattern arising from graphene on Ir(111) has been observed with STM. Atomic resolution was obtained and a graphene monolayer on the Ir(111) surface was visualised.

Hydrogenation of graphene on Ir(111) exposed to vibrationally excited molecules was investigated. Hydrogenation by vibrationally excited molecules was proven successful and the influence of the flux of atomic hydrogen was observed. STM images of the graphene on Ir(111) were created following doses with a hydrogen atomic beam source at temperatures of 1745°C, 1593 °C, and 1343°C. Having a D₂ chamber pressure of $5 \cdot 10^{-7}$ mbar during dosing, it was found that the fraction of hydrogenated moiré super cells after 20 min doses were; 35%, 28%, and a few %. This suggests that a doser temperature of 1343°C produces very few molecules in the $v'' = 7$ state. This agrees with the distribution of atomic hydrogen from the doser shown in chapter 4

STM images revealed that hydrogen preferably adsorbs in the FCC site in the moiré unit cell. However, adsorption in few HCP sites were observed as well. TPD measurements revealed that vibrationally excited molecules lack the energy to form dimers in the ATOP site of the moiré unit cell. Furthermore it was calculated from the TPD measurements that hydrogen adsorbed to graphene on Ir(111) in the HCP and FCC sites has an energy of desorption equal to 2.1 ± 0.4 eV. Graphene bilayers were grown by annealing the sample to temperatures of at least 900°C with an ethylene pressure of $1 \cdot 10^{-6}$ mbar. Fully hydrogenated graphene on Ir(111) surfaces were studied. Using STM it was found that the hydrogenation was absent on the bilayer patches. Furthermore, TPD measurements revealed that a larger number of bilayers on the graphene on Ir(111) surface reduce the maximum amount of hydrogen capable of being stored on the surface.

Furthermore LEED experiments were conducted on the bilayered sample. These revealed that periodic structures were present on the surface. Additionally the LEED experiments indicated that bilayers disappear from the surface as it is annealed to high temperatures above 1000°C.

Conducting TPD measurements at different hydrogenation coverages would provide additional information regarding the dissociation of D₂. From these data it could be determined whether the desorption energy is coverage dependant. This would result in a more precise value than the one given by the Redhead method. Furthermore, TPD measurements at short exposures with a doser temperature of 1343°C would reveal whether the observed structures in the STM images are defects or hydrogenated sites in the moiré unit cell.

Bibliography

- [1] K. S. Novoselov, V. I. Fal[prime]ko, L. Colombo, P. R. Gellert, M. G. Schwab, and K. Kim. A roadmap for graphene. *Nature*, 490(7419):192–200, 10 2012.
- [2] L. Solymar and D. Walsh. *Electrical properties of materials, EIGHTH EDITION*. OXFORD UNIVERSITY PRESS, 2010.
- [3] A. H. Castro Neto, F. Guinea, N. M. R. Peres, K. S. Novoselov, and A. K. Geim. The electronic properties of graphene. *Rev. Mod. Phys.*, 81:109–162, Jan 2009.
- [4] Ludwig A Kibler. Preparation and characterization of noble metal single crystal electrode surfaces. *Short Course Held at the 51st and 53rd Annual Mtg of the ISE*, 2003.
- [5] Alpha T N'Diaye, Johann Coraux, Tim N Plasa, Carsten Busse, and Thomas Michely. Structure of epitaxial graphene on ir(111). *New Journal of Physics*, 10(4):043033, 2008.
- [6] Line Kyhl, Richard Balog, Thierry Angot, Liv Hornekær, and Régis Bisson. Hydrogenated graphene on ir(111): A high-resolution electron energy loss spectroscopy study of the vibrational spectrum. *Phys. Rev. B*, 93:115403, Mar 2016.
- [7] Elena N Voloshina, Edoardo Fertitta, Andreas Garhofer, Florian Mittendorfer, Mikhail Fonin, Andreas Thissen, and Yu S Dedkov. Electronic structure and imaging contrast of graphene moiré on metals. *Scientific reports*, 3, 2013.
- [8] Figure made by line kyhl.
- [9] Richard Balog, Bjarke Jørgensen, Louis Nilsson, Mie Andersen, Emile Rienks, Marco Bianchi, Mattia Fanetti, Erik Laegsgaard, Alessandro Baraldi, Silvano Lizzit, Zeljko Sljivancanin, Flemming Besenbacher, Bjørk Hammer, Thomas G Pedersen, Philip Hofmann, and Liv Hornekaer. Bandgap opening in graphene induced by patterned hydrogen adsorption. *Nature Materials*, 9(4):315–319, 4 2010.
- [10] R. I. Hall, I. Čadež, M. Landau, F. Pichou, and C. Schermann. Vibrational excitation of hydrogen via recombinative desorption of atomic hydrogen gas on a metal surface. *Phys. Rev. Lett.*, 60:337–340, Jan 1988.

- [11] Y. Miura, H. Kasai, W. Diño, H. Nakanishi, and T. Sugimoto. First principles studies for the dissociative adsorption of h₂ on graphene. *Journal of Applied Physics*, 93(6), 2003.
- [12] Line Kyhl, Régis Bisson, Richard Balog, Michael Groves, Andrew Cassidy, Jill Miwa, Jakob Jørgensen, Antonija Grubisic Cabo, Susanne Halkjær, Jan Knudsen, Samuli Urpelainen, Hendrik Bluhm, Thierry Angot, Philip Hofmann, Bjørk Hammer, and Liv Hornekær. Unpublished.
- [13] P. J. Eenshuistra, J. H. M. Bonnie, J. Los, and H. J. Hopman. Observation of exceptionally high vibrational excitation of hydrogen molecules formed by wall recombination. *Phys. Rev. Lett.*, 60:341–344, Jan 1988.
- [14] The aarhus stm. <http://inano.au.dk/research/research-platforms/nanoanalysis/scanning-tunneling-microscopy/>. Accessed: 2016-06.
- [15] Gerd Binnig and Heinrich Rohrer. Scanning tunneling microscopy—from birth to adolescence. *Rev. Mod. Phys.*, 59:615–625, Jul 1987.
- [16] DAWN BONNELL. *Scanning Probe Microscopy and Spectroscopy: Theory, Techniques, and Applications, 2nd Edition*. WILEY-VCH, 2001.
- [17] G. Binnig, H. Rohrer, Ch. Gerber, and E. Weibel. Surface studies by scanning tunneling microscopy. *Phys. Rev. Lett.*, 49:57–61, Jul 1982.
- [18] W.A. Steele, G. Zgrablich, and W. Rudzinski. *Volume 104. Equilibria and Dynamics of Gas Adsorption on Heterogeneous Solid Surfaces*. Elsevier Science, 1996.
- [19] Desorption lecture slides. http://th.fhi-berlin.mpg.de/th/lectures/summer_term_2006/6_desorption.pdf. Accessed: 2016-06.
- [20] Sven L.M. Schroeder and Michael Gottfried. Temperature-programmed desorption (tpd) thermal desorption spectroscopy (tds), 2002.
- [21] Thermal analysis - tds. http://www.fhi-berlin.mpg.de/acnew/department/pages/teaching/pages/teaching__wintersemester__2005_2006/ranke_tds_251105.pdf. Accessed: 2016-06.
- [22] Georg Held. Low-energy electron diffraction. 1974.
- [23] Surface chemistry. <http://www.chemistryexplained.com/St-Te/Surface-Chemistry.html>. Accessed: 2016-06.
- [24] Technical information data bulletin, type k thermocouple, chromel-alumel. http://www.tnp-instruments.com/sitebuildercontent/sitebuilderfiles/type_kc_table.pdf. Accessed: 2016-06.
- [25] Hydrogen atom beam source - datasheet. <http://www.mbe-komponenten.de/products/pdf/data-sheet-habs.pdf>. Accessed: 2016-06.

- [26] Revised thermocouple reference tables, type c. http://www.src.wisc.edu/users/scienta_info/Scientia_200U/Reference%20Material/Type%20C%20Thermocouple%20Table.pdf. Accessed: 2016-06.
- [27] KG Tschersich. Intensity of a source of atomic hydrogen based on a hot capillary. *Journal of Applied Physics*, 87(5):2565–2573, 2000.
- [28] Johann Coraux, Alpha T N'Diaye, Martin Engler, Carsten Busse, Dirk Wall, Niemma Buckanie, Frank-J Meyer zu Heringdorf, Raoul van Gastel, Bene Poelsema, and Thomas Michely. Growth of graphene on ir(111). *New Journal of Physics*, 11(2):023006, 2009.
- [29] Pyrometer handbook. Work of IMPAC Infrared GmbH. 2004.
- [30] Johann Coraux, Alpha T N'Diaye, Carsten Busse, and Thomas Michely. Structural coherency of graphene on ir (111). *Nano letters*, 8(2):565–570, 2008.
- [31] Jakob Jørgensen, Antonija Grubisic Cabo, Line Kyhl Hansen, Richard Balog, Philip Hofmann, and Liv Hornekær. Unpublished.
- [32] Richard Balog, Mie Andersen, Bjarke Jørgensen, Zeljko Sljivancanin, Bjørk Hammer, Alessandro Baraldi, Rosanna Larciprete, Philip Hofmann, Liv Hornekær, and Silvano Lizzit. Controlling hydrogenation of graphene on ir (111). *ACS nano*, 7(5):3823–3832, 2013.
- [33] Mie Andersn. Unpublished.
- [34] Liv Hornekær, Ž Šljivančanin, W Xu, R Otero, E Rauls, Ivan Stensgaard, Erik Lægsgaard, Bjørk Hammer, and Flemming Besenbacher. Metastable structures and recombination pathways for atomic hydrogen on the graphite (0001) surface. *Physical review letters*, 96(15):156104, 2006.
- [35] J. Červenka and C. F. J. Flipse. Structural and electronic properties of grain boundaries in graphite: Planes of periodically distributed point defects. *Phys. Rev. B*, 79:195429, May 2009.
- [36] Leed performed by antonija grubisic cabo.
- [37] J. Tersoff and D. R. Hamann. Theory and application for the scanning tunneling microscope. *Phys. Rev. Lett.*, 50:1998–2001, Jun 1983.